https://doi.org/10.1016/j.compstruct.2020.112552

Strengthening of RC beams with rectangular web openings using externally bonded FRP: numerical simulation

X.F. Nie[1], S.S. Zhang[2, *], G.M. Chen[3] and T. Yu[4]

[1] Post-doctoral Fellow, School of Civil Engineering and Mechanics, Huazhong University of Science and Technology, Wuhan 430074, China.
[2] Professor, School of Civil Engineering and Mechanics, Huazhong University of Science and Technology, Wuhan 430074, China.
[3] Professor, State Key Laboratory of Subtropical Building Science, South China University of Technology, Guangzhou 510641, China.
[4] Professor, Department of Civil and Environmental Engineering, The Hong Kong Polytechnic University, Hung Hom, Kowloon, Hong Kong, China.

Abstract: Making web openings in reinforced concrete (RC) beams is frequently required for the passage of utility ducts and/or pipes. Such web opening(s) leads to reduction of the strength and stiffness of the beam. To ensure the safety of the beam, a strengthening system applied around the web opening is needed. Existing experimental studies have confirmed the feasibility of using externally bonded FRP to compensate for the strength loss of the beams caused by the creation of web openings, while there have been very limited finite element (FE) approaches for predicting the behavior of such RC beams. Against this background, three alternative FE models developed using ABAQUS for the simulation of RC beams with an FRP-strengthened rectangular web opening are presented in this paper, including two models based on the brittle cracking model of concrete and one model based on the concrete damaged plasticity model. By comparing their predictions with test results collected from the published literature, the most proper FE approach is identified. By using this FE approach, parametric studies are conducted for the design of the FRP-strengthening system for a typical web opening-weakened RC beam, and a reliable FRP-strengthening system is recommended for use in practice.

Keywords: reinforced concrete (RC) beam; web opening; fiber-reinforced polymer (FRP) strengthening; finite element (FE) model; concrete cracking; dynamic analysis approach

* Corresponding author, S.S. Zhang, Email: shishun@hust.edu.cn

1. INTRODUCTION

In new reinforced concrete (RC) structures, pre-formed web openings in the beams have been widely used for the passage of utility ducts/pipes, such as electricity, heating and water supply systems as well as air conditioning, telephone, internet cables and sewage conduits [e.g. 1-3]. Such web openings help avoid extra storey heights for accommodating the ducts/pipes and thus reduce the overall height of the building, leading to reduction of the loads on the load-carrying structural members and foundation and then the achievement of a more economical design of the building. To prevent/mitigate the associated performance degradation of the RC beams due to the presence of web openings, the beams are usually reinforced using steel reinforcement around the web openings [1-3]. It should be stated that, as the web openings are generally far apart and do not interact with each other, RC beams with one or more such openings are referred to as "beams with a web opening" or "beams with an opening" for simplicity hereinafter, regardless of the number of openings.

In existing RC structures, if such ducts/pipes are required but there are no pre-formed web openings in the beams for such a purpose, creating web openings in the beams is an attractive solution and has already been adopted in real projects [e.g. 4-6]. Nevertheless, the creation of such a web opening in an existing RC beam leads to reduction of cross sectional area and severing of some of the existing shear reinforcement of the beam, and thus reduction of the shear capacity and stiffness of the beam [e.g. 4-6]. To ensure the safety of the beam, a strengthening system [such as an externally bonded fibre-reinforced polymer (FRP) strengthening system] needs to be applied around the post-formed web opening (referred to as "web opening" hereafter in this paper) [e.g. 4-6]. Externally bonded FRP reinforcement has been shown by many researchers to be an effective way to enhance the flexural/shear capacity of RC beams [e.g. 7-9]. A number of experimental studies on the behavior of RC beams with an FRP-strengthened web opening have confirmed the significant strength reduction due to the creation of an opening in the beam and the feasibility of FRP strengthening to compensate for the weakening effect of the opening [e.g. 4-6].

The existing experimental studies have provided useful information on the performance of RC beams with an FRP-strengthened web opening. Nevertheless, there is no reliable method for predicting the behavior of such RC beams by now, and a reliable design method for the FRP-strengthening systems of such beams is still lacking. While experimental studies are essential in understanding the structural behavior of RC beams with an FRP-strengthened web opening, a finite element (FE) model can serve as a powerful and economical alternative to laboratory testing. A proper FE model can be used to better or more efficiently examine many behavioral aspects of such beams (e.g., strength, stiffness and crack development), and furthermore it can be adopted for the design of the associated FRP-strengthening systems. For FRP-strengthened RC beams without a web opening, a number of numerical studies have been conducted [e.g. 10-15]. However, up to now, studies on FE modelling of RC beams with an FRP-strengthened web opening [16-18] are very limited and have not led to a reliable FE approach. The study presented in this paper was conducted to develop such an FE approach with the general purpose package ABAQUS [19].

Nie [20] conducted a study on the FE modelling of RC beams with an un-strengthened web opening through the dynamic analysis approach using ABAQUS

[19]. Through comparing the predictions of the three proposed FE approaches investigated in Ref. [20] with the test results, the most reliable approach was finally identified and recommended for the simulation of RC beams with an un-strengthened web opening. In the present study, the proposed FE approaches in Ref. [20] were further developed through incorporating proper bond-slip relationship for modelling the bond behavior between externally-bonded FRP and concrete, to simulate RC beams with an FRP-strengthened web opening. Based on the comparison between predictions and test results collected from the published literature, the proper FE approach for such modelling is determined. Furthermore, existing FRP-strengthening schemes adopted by the researchers for the web opening-weakened RC beams are comprehensively reviewed, and then parametric studies are conducted using the determined FE approach for the design of FRP-strengthening system for a typical web opening-weakened RC beam in order to study the effectiveness of different FRP-strengthening schemes. It should be noted that although the present study was conducted on RC beams with an FRP-strengthened rectangular web opening, the conclusions are also largely applicable to RC beams with an FRP-strengthened web opening of other shapes (e.g. a circular web opening).

2. EXISTING STUDIES ON RC BEAMS WITH AN FRP-STRENGTHENED WEB OPENING

The present study is focused on RC beams with an FRP-strengthened web opening in which the web opening is post-formed to meet the new functional requirements (e.g. passage of pipe systems). In order to provide the necessary background for the present study, the relevant existing experimental and numerical studies are summarised below.

2.1. Experimental studies

A total of nine experimental studies in the published literature [4-6, 16, 17, 21-24] have addressed the effect of drilling an opening in an existing beam and the effectiveness of the associated strengthening measure; all nine studies except the one by Suresh and Prabhavathy [23] proposed the use of externally bonded FRP reinforcement for the strengthening of the web opening. The first of these studies was conducted by Mansur et al. [4], in which three T-section RC beams were tested. One of the three beams had no web openings and served as the control specimen, while the other two beams had a circular web opening in each shear span. One of these two beams with a web opening was un-strengthened while the other one was strengthened using bonded FRP plates around the web opening on each side of the beam. The control beam failed by the crushing of the compressive concrete, which is a typical flexural failure mode; the beam with an un-strengthened circular web opening failed by the formation and propagation of a diagonal shear crack in each shear span passing through the circular opening; and the beam with an FRP-strengthened circular web opening failed in a flexural mode due to the crushing of the compressive concrete at mid-span. Nearly all the subsequent studies on this topic were concerned with rectangular RC beams with an FRP-strengthened rectangular opening [5, 6, 17, 21, 22, 24], with the parameters examined mainly being the size of the opening and with or without (w or w/o) FRP-strengthening. Most of these studies tested beams with two web openings of the same size symmetrically located in the two shear spans respectively [4, 5, 16, 17, 24], while a smaller number of studies tested beams which had only one web opening in one of the two shear spans [6, 21, 22]. As mentioned earlier, all these beams are referred to as “beams with a web opening” or “beams with an opening" regardless of the number of openings, unless when the number of openings is important.

Six main FRP-strengthening schemes have been proposed in these existing experimental studies and the corresponding schematics are shown in Fig.1: (1) vertically bonded FRP U-jackets on the chords [5, 6, 22] or on the two sides of the opening [6] (Fig. 1a); (2) vertically bonded FRP complete wraps on the chords [5, 6] or on the two sides of the opening [21] (Fig. 1b); (3) vertical side-bonded FRP sheets/plates on the two sides of the opening [5, 17, 21, 22] (Fig. 1c); (4) diagonal side-bonded FRP plates near the corners of the opening [4] (Fig. 1d); (5) horizontally bonded FRP sheets/plates on the side surfaces of the chords [4-6, 17, 21, 22, 24] or on the top and bottom surfaces of the beam [17] (Fig. 1e); and (6) diagonal near-surface mounted FRP bars near the corners of the opening [16] (Fig. 1f). The above listed strengthening schemes were adopted individually or combined by the researchers. For example, Maaddawy and Ariss [6] used FRP U-jackets on the top chord, FRP complete wraps on the bottom chord, vertical side-bonded FRP sheets on the two sides of the opening and horizontally bonded FRP sheets on the side surfaces of two chords together to strengthen their beams with a web opening; while the beam with a web opening tested by Chin et al. [24] was strengthened only by horizontally bonded FRP plates on the side surfaces of the chords. The figures showing the detailed FRP-strengthening schemes adopted in these studies are not shown in the present paper to avoid copyright complications. For more details, the reader is referred to the original sources. The above summarised FRP-strengthening schemes were found to be effective in preventing/mitigating shear cracks initiating from the corners of the web opening and compensating for the weakening effect of the opening. However, it should be noted that some of these FRP-strengthening schemes (e.g., vertically bonded FRP complete wraps on the top chord or on the two sides of the opening) are only applicable to RC beams without floor slabs; if such FRP-strengthening schemes need to be applied on RC beams with floor slabs, slits need to be cut in the slabs, which might involve a complex application process.

In addition to the existing published studies on this topic, the authors' group conducted a test on a T-section beam with an FRP-strengthened rectangular opening in one of the two shear spans to further investigate the behavior of such RC beams [25]. The layout of the tested beam is shown in Fig. 2. In the test, the beam had a height of 500 mm, a web width of 250 mm, a flange thickness of 100 mm, a total flange width of 1,450 mm, a beam clear span of 3,300 mm, a shear span of 1,650 mm and a rectangular opening of 500 mm (length) × 220 mm (height).

A summary of the existing experimental studies on RC beams with an FRP-strengthened web opening together with the test carried out by the authors' group [25] is given in Table 1. It can be indicated from Table 1 that although the size and type of the beam (rectangular or T-section), the size and number of openings, and the FRP-strengthening schemes adopted in these studies vary from one to another, the following observations can be summarised based on the existing studies:

1) All control beams without a web opening failed in a typical flexural failure mode of RC beams (i.e. the crushing of compressive concrete at the mid-span of the beam);
2) All RC beams with an un-strengthened web opening failed in a shear mode due to the formation and propagation of a diagonal crack that started as small inclined cracks near the corners of the opening; all RC beams with an FRP-strengthened web opening failed by shear in the opening region after the debonding/rupture of FRP, except the beams tested by Mansur et al. [4], Abdalla et al. [21] and Pimanmas [16], which failed in a flexural mode as the opening size was quite small; and
3) A web opening/web openings significantly reduced both the strength and stiffness of the beam; after FRP-strengthening, the strength of the beam can be substantially restored.

2.2. Finite element modelling

In studying the behavior of concrete structures, FE modelling is an efficient and cost-effective alternative to laboratory testing, as laboratory tests are usually time-consuming and costly. However, most of the existing studies on RC beams with an FRP-strengthened web opening were experimentally based, and only a very limited amount of studies were based on the numerical simulation using the FE approach. Only three relevant numerical studies can be found in the open literature [16-18].

Based on the smeared crack approach, Pimanmas [16] conducted 2-dimentional (2D) nonlinear FE analyses of RC beams with a rectangular web opening using the nonlinear FE program WCOMD [26]. The beams tested in his study were strengthened using diagonal near-surface mounted FRP bars near corners of the opening. Chin et al. [17] presented 2D FE studies of RC beams with a rectangular web opening which were strengthened using externally bonded FRP sheets and wraps. The general purpose FE program ATENA [27] was adopted in their study. By using ANSYS [28], Hawileh et al. [18] proposed a 3-dimentional (3D) nonlinear FE model for deep RC beams with a rectangular web opening which were strengthened using externally bonded FRP sheets and wraps.

The details of the three existing numerical studies on RC beams with an FRP-strengthened web opening are summarized in Table 2 to emphasize their differences and inadequacies. As can be seen from Table 2, none of the three FE studies accurately modelled the bond-slip behavior between steel and concrete, and instead, a perfect bond was assumed. Besides, Pimanmas's model [16] did not include accurate modelling of the bond-slip behavior between FRP and concrete, and also, a perfect bond was assumed instead. The perfect bond assumption will cause inaccurate predictions of the crack patterns [29]. Furthermore, none of the three FE studies accurately simulated the behavior of cracked concrete. The tensile fracture energy in the simulation of the tensile behavior of cracked concrete was not considered in the approaches proposed by Pimanmas [16] and Hawileh et al. [18], which implied that the predictions of the FE models could be mesh-dependent. Finally, the accuracies of the existing FE models need to be verified by using a larger test database which also contained test results from other researchers. Therefore, based on the above analyses of the limited existing numerical studies on RC beams with an FRP-strengthened web opening, it can be concluded that a proper FE approach for predicting the behavior of such RC beams has not been well-established, which indicates that the study presented in this paper is quite necessary.

3. PROPOSED FINITE ELEMENT APPROACH

3.1. FE meshes

A 2D FE model for RC beams with an FRP-strengthened web opening established using the general purpose FE program ABAQUS [19] was proposed in the present study. It should be noted that this paper only focuses on RC beams with a rectangular web opening strengthened using externally bonded FRP, which was most commonly used in the relevant existing experimental studies. In the proposed FE model, the concrete was simulated using 4-node plane stress elements CPS4R, and both the steel bars and the externally bonded FRP were simulated using 2-node truss elements T2D2. For the modelling of externally bonded FRP, the 2-node truss elements were arranged in the fiber direction of the FRP, and the cross-sectional areas of truss elements were determined by the thickness of the FRP and the spacing of the truss elements (i.e., the width of the corresponding concrete elements). For FRP U-jackets, one end of the lowest FRP truss elements (i.e., nearest to the soffit of the beam) was fixed onto the bottom surface of the beam (i.e. to the corresponding concrete node). For FRP complete wraps, one end of the lowest FRP truss elements was fixed onto the bottom surface of the beam, while one end of the highest FRP truss elements (i.e., nearest to the top surface of the beam) was fixed onto the top surface of the beam. The bond behavior between concrete and both steel reinforcement (longitudinal bars and stirrups) and externally bonded FRP was modelled using 4-node interfacial elements COH2D4. All the elements employed a reduced integration scheme. The typical meshes are shown in Fig. 3. Based on the results of a convergence study, the side length of most concrete elements was determined to be 10 mm, with the side length of some concrete elements being appropriately adjusted in the vertical direction under the level of steel tension bars. A maximum of one steel/FRP element would exist between two adjacent concrete element nodes, and thus the size of steel/FRP element was determined (i.e. all steel/FRP elements had a length of 10 mm). The applied boundary conditions and loads are shown in Fig. 3. In order to prevent premature local failure of concrete at the two supports and the loading point/points, six elastic elements with the same elastic modulus as the concrete were placed near each support and the loading point/points respectively to simulate the rubber pads which were normally used in the tests. Then the displacement restraints at the two supports and imposed displacement at the loading point/points were applied through these elastic elements, as shown in Fig. 3.

3.2. Constitutive modelling of concrete

For the accurate prediction of the behavior of RC beams with an FRP-strengthened web opening, the accurate simulation of the cracked concrete (especially the tensile and shear behavior of the cracked concrete) is one of the most important factors. In the present study, the crack band concept [30] and the fracture energy given by CEB-FIP [31] were adopted for the simulation of the cracked concrete.

Two concrete crack models available in ABAQUS/Explicit (i.e. the concrete damaged plasticity model and the brittle cracking model) were examined in this study. The concrete damaged plasticity model adopts concepts of combining isotropic damaged elasticity with isotropic compressive and tensile plasticity to simulate the inelastic behavior of concrete, while the brittle cracking model is more competitive in applications in which the brittle cracking behavior (tensile and shear behavior) of concrete plays a leading role [19]. These two models have the potential to achieve accurate simulation of cracked concrete and thus were both investigated in this study for the purposes of comparison. It should be noted that due to the space limitation, the relevant equations of the constitutive models of concrete and bi-material bond-slip models are given in Appendix A.

3.2.1. Brittle cracking model

The brittle cracking model is proposed for simulations of structures whose behavior is dominated by the tensile and shear behavior of concrete, and therefore the compressive behavior of concrete is assumed to be linear elastic in the brittle cracking model.

Tension-softening curve of cracked concrete

To model the behavior of cracked concrete in tension, the exponential tension-softening curve of concrete proposed by Hordijk [32] (Eq. A1 in Appendix A) was adopted, following Chen et al.'s studies [29, 33]. It should be noted that, in the brittle cracking model, the concrete is assumed to be linear elastic before reaching its tensile strength (i.e., before initiation of cracking). However, before reaching the tensile strength of concrete, the actual tensile stress-strain curve of concrete is not linear. Actually, the modulus (slope of the tensile stress-strain curve) decreases constantly as the tensile stress increases, as shown in Fig. 4 [34]. Therefore, it might not be reasonable to use the initial elastic modulus of concrete (e.g. $E_0 = 4730\sqrt{f_c}$ according to ACI-318 [35], where both E_0 and f_c are in *MPa*). Against this reason, both the initial elastic modulus and the secant modulus (defined as the ratio between the maximum tensile stress and the corresponding tensile strain of concrete, i.e., $\sigma_{to}/\varepsilon_{to}$ shown in Fig. 4) of concrete were adopted to define the brittle cracking model in later studies for comparison purposes. In the present study, it was assumed that the secant modulus of concrete is half of its initial elastic modulus, following the studies of Ye [34] and Pimanmas [16].

<u>*Shear retention factor model of cracked concrete*</u>

In the present study, Rots's model [36] (Eq. A5 in Appendix A) was employed to define the shear retention factor (β_s), which reflects the shear stress-strain (or slip) relationship of concrete after cracking. The details of this model are given in Appendix A.

3.2.2. Concrete damaged plasticity model

<u>*Compressive behavior of concrete*</u>

Following Chen et al.'s study [33], the inelastic behavior of concrete in compression can be simulated using the concrete damaged plasticity model. In the present study, the uniaxial compressive stress-strain curve proposed by Saenz [37] (Eq. A6 in Appendix A) was adopted, and the details are given in Appendix A.

<u>*Tensile and shear behavior of concrete*</u>

In the present study, the same tension-softening curve and shear retention factor model of cracked concrete employed in the brittle cracking model (i.e., expressed in Eqs. A1 to A5 in Appendix A) were also adopted in the concrete damaged plasticity model. The corresponding stiffness degradation variable of cracked concrete (d_t) can be determined through Eq. A7 in Appendix A.

3.3. Modelling of steel bars and bond behavior between steel and concrete

The steel bars which include the steel tension bars, steel compression bars and stirrups were simulated as an elastic-perfectly plastic material. In the present study, relative displacements in the normal direction are not allowed between steel bars and concrete, and thus the normal stiffness between steel bars and concrete was simply assumed to be infinite. In the shear direction, the bond-slip model of CEB-FIP [31] (Eq. A8 in Appendix A) was employed to simulate the shear bond behavior between steel bars and concrete.

3.4. Modelling of FRP and bond behavior between FRP and concrete

In the present study, the externally bonded FRP reinforcement was assumed to be linear-elastic-brittle. The bond-slip model for externally bonded FRP reinforcement proposed by Lu et al. [39] (Eq. A9 in Appendix A) was adopted to simulate the bond behavior between FRP and concrete in the shear direction. This bond-slip model consists of an ascending branch with continuous stiffness degradation and a descending branch which drops to zero bond stress when the slip is sufficiently large. This bond-slip relationship has been successfully used by Chen et al. [33] and many others [e.g. 12, 29, 40] in the modelling of RC beams strengthened with externally bonded FRP reinforcement, and is thus expected to be able to give accurate predictions in the present modelling work.

In the normal direction of the FRP-to-concrete interface, the interfacial elements were assumed to be linear-elastic with a very large stiffness, which was based on the assumption that the interaction of bond between the normal and shear directions is insignificant and can be ignored, and the debonding between FRP and concrete depends only on the bond-slip behavior parallel to the FRP-to-concrete bonded interface.

3.5. Dynamic analysis approach

In order to overcome the serious numerical convergence difficulties which are commonly encountered in the simulation of crack concrete by using static analysis approaches (e.g., the Newton-Raphson method or the arc-length method), the dynamic analysis approach (i.e., the explicit central difference method available in ABAQUS) instead of the static analysis approach was adopted in the present study, following Chen et al.'s study [41]. An advanced dynamic approach was proposed by Chen et al. [41] to solve static/quasi-static structural problems, which provides a solid basis for the present study. As suggested by Chen et al. [41], when the explicit central difference method is employed in the dynamic approach, key elements including the damping scheme and the loading time should be carefully selected to achieve accurate/reliable predictions.

Following the suggestion by Chen et al. [41], the stiffness-proportional Rayleigh damping matrix C, which can be expressed as $C=\beta K$ (K is the stiffness matrix and β is the damping factor to be defined in the FE model) [42], was adopted in the FE approach. If the damping factor β is too small, the dynamic effects cannot be effectively damped out and therefore large fluctuations will exist in the predicted load-deflection curves; while if the damping factor β is too large, the damping forces which are proportional to damping ($C\dot{d}$, where $\dot{d}$ is velocity) will be too high, and thus the ultimate load will be significantly overestimated.

Loading rate, which is defined as the ratio (d/t) of the applied maximum displacement (d) to the loading time (t), is determined by the loading time when a certain displacement is specified. If the loading rate is too high, the goal of conducting a quasi-static analysis might not be achieved as the dynamic response of the beam cannot be ignored; while if the loading rate is too low, a much heavier computing effort and much larger accumulated errors (due to the explicit nature of the central difference method) will be involved [41]. Against the above analyses, optimal damping factor β and loading time t need to be carefully determined.

3.6. Examined schemes

In the FE analyses, the damping factor β was chosen to be 1×10^{-5}, and the loading time was chosen to be $50T_1$ (where T_1 is the period of the fundamental vibration mode of the beam and can be found from an eigenvalue analysis of the FE model), following Nie's study [20]. The values of the period of the fundamental vibration mode (T_1) of the collected and simulated specimens are listed in Table 3. The exponent n in the shear retention factor model (Eq. A5 in Appendix A) was chosen to be 5 for the brittle cracking model following Nie's study [20] and also 5 for the concrete damaged plasticity model following Chen et al.'s study [29]. For comparison purposes, three schemes were examined in the present study: (1) Scheme-1: the brittle cracking model, with the secant modulus of concrete recommended by Ye [34] and Pimanmas [16] (i.e. equal to half of the initial elastic modulus of concrete) being adopted, was employed to simulate cracked concrete (referred to as the ***BC model with SECANT modulus*** hereinafter for simplicity); (2) Scheme-2: the brittle cracking model, with the initial elastic modulus of concrete given by ACI-318 [35] being adopted, was employed to simulate cracked concrete (referred to as the ***BC model with INITIAL modulus*** hereinafter for simplicity); and (3) Scheme-3: the concrete damaged plasticity model was employed to simulate the behavior of cracked concrete (referred to as the ***DP model*** hereinafter for simplicity).

4. RESULTS AND COMPARISON

4.1. Test database

A total of 12 RC beams with an FRP-strengthened web opening were collected from the existing experimental studies to verify the accuracy of the proposed FE approach. These test beams were chosen because sufficient geometric and material properties had been provided. As mentioned earlier, the present study is only concerned with RC beams with a rectangular web opening strengthened with externally bonded FRP. Therefore, the specimens tested by Mansur et al. [4] in which the web opening was circular and the specimens tested by Pimanmas [16] which were strengthened using diagonal near-surface mounted FRP bars at the opening corners are out of the scope of present study. Moreover, the specimens tested by Maaddawy and Sherif [5] (very deep beams with a shear span ratio of 0.8) were also not considered in the comparison, due to the following reasons: (1) very deep RC beams (with a shear span ratio of less than 1) are much less often used in practice compared with RC beams with a larger shear span ratio; and (2) the behavior of such beams, whose failure is dominated by the compression failure of concrete, is much different from RC beams with a larger shear span ratio in which the tensile and shear behavior of concrete plays an important role. As a result, the findings from the present study is only applicable to RC beams with a shear span ratio of lager than 1. Details of the collected specimens are given in Table 4 and material properties of the collected specimens are given in Table 5.

4.2. Load-deflection curves

The load-deflection curves obtained from the three examined schemes are compared with the test results in Fig. 5. As can be seen from Fig. 5, for all 12 specimens tested by Maaddawy and Ariss [6], Abdalla et al. [21], Allam [22], Chin et al. [17], Chin et al. [24] and Teng et al. [25], the brittle cracking model with SECANT modulus gives the most accurate predictions of the load-deflection curves in terms of both the predicted ultimate load and the stiffness. The brittle cracking model with INITIAL modulus consistently overestimates the ultimate load as well as the stiffness of the beam, while the DP model usually significantly underestimates the ultimate load but overestimates the stiffness.

A comparison of the ultimate loads between FE analyses and tests for all the collected specimens are given in Fig. 6 and Table 6. As can be seen from Fig. 6 and Table 6, the brittle cracking model with SECANT modulus gives closest predictions of the ultimate loads from tests, with an average prediction-to-test ratio of 1.00, a standard deviation (STD) of 0.0848, and a coefficient of variation (CoV) of 0.0845. On the contrary, the brittle cracking model with INITIAL modulus substantially overestimates the ultimate load, with an average prediction-to-test ratio of 1.17, a STD of 0.175, and a CoV of 0.150; the DP model significantly underestimates the ultimate load, with an average prediction-to-test ratio of 0.796, a STD of 0.228, and a CoV of 0.287. The better performance of the brittle cracking model with SECANT modulus is also evidenced by the much smaller scatter in its predictions of test results as shown in Fig. 6. It can be therefore concluded that the brittle cracking model with the secant modulus of concrete performs much better than the concrete damaged plasticity model for the simulation of RC structures whose failure is governed by the tensile and shear behavior of cracked concrete rather than the compressive behavior of concrete. Moreover, the better performance of the brittle cracking model with the secant modulus of concrete than the brittle cracking model with the initial modulus of concrete can be attributed to the following reason: as can be seen from Fig. 4, the ascending branch of the tensile stress-strain curve of concrete is nonlinear, and the initial modulus of concrete is only available for a very small portion of the curve at the initial stage; in contrast, the adoption of secant modulus can give a much closer prediction of the tensile stress-strain curve of concrete, with only slightly underestimating the stiffness of the ascending branch.

4.3. The initiation of FRP debonding

For RC beams with an FRP-strengthened web opening, the initiation of FRP debonding commonly occurs at the corners of the opening due to the development of inclined cracks initiating at these regions. The adopted dynamic analysis approach can not only overcome the severe numerical convergence difficulties commonly encountered in the modelling of cracked concrete using static analysis approaches, but also capture the local dynamic responses caused by a sudden release of energy, such as the initiation and development of FRP debonding. Therefore, the development history of the kinetic energy during the whole loading process of the specimen, which can be directly obtained from the Output of Abaqus/CAE, was examined to identify the initiation of FRP debonding in the present study. The kinetic energy is defined in

ABAQUS [19] as $\int \frac{1}{2} \rho v \cdot v dV$ (ρ is the mass density, v is the velocity field vector, and V is the volume) and thus reflects the dynamic/strain rate-dependant responses of the beam. Specimen S1-500×120 tested by Maaddawy and Ariss [6] was selected as an example to illustrate the detailed process, as its test results were clearly reported. The predicted development history of the kinetic energy using the brittle cracking model with SECANT modulus is plotted in logarithmic scale in Fig. 7, in which the test and predicted load-deflection curves are also shown for reference. As shown in Fig. 7, the kinetic energy remains in a low range at the early loading stage, and experiences a sudden increase at a deflection of 8.6 mm. Such a sudden increase indicates the initiation of FRP debonding. Afterwards, the kinetic energy starts fluctuating, caused by the gradual debonding of FRP. When the deflection further increases to about 12 mm, the kinetic energy steps into a higher level and fluctuation becomes more severe, which indicates that failure of the beam happens. The development of the kinetic energy reflects well the changes in the predicted load-deflection curve. As shown in Fig. 7, the predicted load-deflection curve keeps ascending at the early loading stage and achieves a local peak value at the deflection of 8.6 mm, corresponding to the initiation of FRP debonding. When the deflection further increases to about 12 mm, the load experiences a sudden drop, indicating the failure of the beam. The initiation of FRP debonding predicted by the FE analysis is marked by a circle in the predicted load-deflection curve, and the initiation of FRP debonding obtained from test [6] is marked by a square in the test load-deflection curve, as shown in Fig. 7. It can be seen from Fig. 7 that the predicted and test points of initiation of FRP debonding are quite close to each other.

The predicted points of the initiation of FRP debonding of the collected specimens are shown in Fig. 8, in which the test points of initiation of FRP debonding are also shown for comparison if they were reported in the relevant publications. As can be seen from Fig. 8, the predicted and the test points of initiation of FRP debonding are very close to each other for all the compared specimens.

4.4. Failure process and failure mode

The failure mode of Specimen FRP-500×220 (T-section beam) tested by the authors' group [25] was recorded in detail and available to the authors, thus this specimen was selected as the example in the comparison of failure process and failure mode between test and prediction obtained from the brittle cracking model with SECANT modulus.

The failure mode of the specimen is shown in Fig. 9, from which it can be seen that the failure of the beam was dominated by the debonding of CFRP U-jackets on the opening side closer to the loading point. After removing the debonded CFRP U-jackets, an inclined crack (around 45 degrees above the horizontal direction), which initiated from the opening corner nearest to the loading point and extended to the loading point, was found (Fig. 9b). In addition, flexural cracks were observed in the flange chord near both its bottom surface (closer to the loading point, as shown in Fig. 9c) and its top surface (closer to the corresponding support, as shown in Fig. 9d).

The predicted crack patterns (represented by the maximum principal cracking strain) of Specimen FRP-500×220 at different load levels are shown in Fig. 10. As can be seen from Fig. 10, when the load reaches 110 kN, an inclined crack (around 45 degrees above the horizontal direction) occurs at the opening corner closest to the loading point. Meanwhile, one flexural crack occurs at one end (closer to the loading point) of the flange chord near its bottom surface, while another one occurs at the other end (i.e., closer to the corresponding support) of the flange chord near its top surface (Fig. 10a). At the load of 224 kN, a major flexural crack forms at the mid-span of the beam (Fig. 10b). As the load increases to higher levels, the existing cracks become wider, and at the same time, shear cracks gradually appear in the shear span of the beam without a web opening. When the load reaches 384 kN, a large inclined crack forms near the top corner of the web opening nearer to the support (Fig. 10c). When the load further increases to 455 kN, the failure of the beam is achieved. The inclined crack at the opening corner closest to the loading point which reaches the loading point can be obviously seen (Fig. 10d). A comparison between Fig. 10d and Fig. 9 shows that the predicted crack pattern of the beam agrees well with the observation in the test.

The predicted crack patterns at failure of the other 11 collected specimens by using the brittle cracking model with SECANT modulus are plotted in Fig. 11. As can be seen from Fig. 11, at failure of the specimens, substantial shear cracks are formed near the corners of the web opening. The predicted crack patterns also agree well with the test observations, which are not shown in the present paper to avoid copyright complications. For more details, the reader is referred to the original sources.

4.5. Comparison between un-strengthened and FRP-strengthened beams

The test and predicted (using the brittle cracking model with SECANT modulus) load-deflection curves of the RC beams with an un-strengthened web opening [20] and the corresponding beams with an FRP-strengthened web opening are plotted in Fig. 8. As can be seen from Fig. 8, after FRP strengthening, both the predicted strength and stiffness of the beam increase, which is as expected and as observed in the tests. In addition, it can also be seen from Fig. 8 that the agreement between predictions and tests is better for RC beams with an FRP-strengthened web opening than for the corresponding specimens with an un-strengthened web opening. This might be because that FRP strengthening can mitigate the scatter of the test results caused by the relatively large scatter of the material property of concrete.

Specimens CN-500 × 120 (un-strengthened beam) and S1-500 × 120 (FRP-strengthened beam) tested by Maaddawy and Ariss [6] were taken as examples to illustrate the effect of FRP strengthening on the crack patterns, as shown in Fig. 12. As can be seen from Fig. 12, after FRP strengthening, the development of the localized cracks near the corners of the web opening are well restricted by the FRP and thus forced into a larger region of the beam.

5. DESIGN OF THE FRP-STRENGTHENING SYSTEM

On the basis of the above analyses, the brittle cracking model with SECANT modulus provides the best predictions of the existing test beams, and is thus recommended for use in the simulation of RC beams with an FRP-strengthened web opening. As reviewed in Section 2.1, different FRP-strengthening schemes have been proposed in the existing experimental studies. However, the effectiveness of these different FRP-strengthening schemes has not been compared, and proper design method for the FRP-strengthening system has not been proposed. In this section, the recommended FE approach (i.e. the brittle cracking model with SECANT modulus) is used to design the FRP-strengthening system for a typical weakened RC beam by the creation of a web opening. Specimens tested by Allam [22] were taken as examples to illustrate the detailed design process, as the web opening size adopted in this study is relatively large (i.e. the weakening effect of the web opening on the beam is great), and the stirrups interrupted by the web opening were still remaining in the beams, which accorded with the actual situation but was ignored in some relevant studies [e.g. 6]. Four RC rectangular beams, with a height of 400 mm, a width of 150 mm, a total length of 3200 mm, a beam clear span of 3,000 mm and a shear span of 1,000 mm, were tested under four-point bending by Allam [22]: one beam (B1) had no web opening and served as the control beam, and the other three beams had a rectangular web opening (opening width × height being 450 mm × 150 mm) in one of the two shear spans. The opening was located at a distance of 300 mm from the closer support. The height of the bottom chord was 100 mm and that of the top chord was 150 mm. One of the three beams with a web opening was un-strengthened (B2) while the other two beams (B8 and B9) were strengthened using externally bonded FRP. Specimen B8 was strengthened using externally bonded one-layer horizontal CFRP sheet on the side surfaces of top and bottom chords (as the diagram shown in Fig. 1e) and one-layer vertical CFRP sheet on the two sides of the opening (as the diagram shown in Fig. 1c). In addition to the strengthening schemes adopted in Specimen B8, additional one-layer vertical CFRP U-jacket on the top and bottom chords and one-layer horizontal CFRP U-jacket on the two sides of the opening were applied in Specimen B9. The control beam B1 failed in a flexural mode due the crushing of the compressive concrete; Specimen B2 failed by shear due to the formation and propagation of diagonal shear cracks in the opening corners; Specimens B8 and B9 failed by shear at the opening region after debonding of FRP. For more details, the reader is referred to the original source. The present simulation was conducted based on the un-strengthened beam B2.

The strengthening schemes examined in the present study included externally bonded horizontal CFRP sheets on the side surfaces of top and bottom chords (Fig. 1e), vertical side-bonded CFRP sheets (Fig. 1c)/CFRP U-jackets (Fig. 1a)/CFRP wraps (Fig. 1b) on the two sides of the opening or the top and bottom chords, and the combination of the above schemes. These strengthening schemes were chosen because they can effectively restrict the development of cracks in the opening region. The same CFRP used in Allam's study [22] was adopted in the present study. The material properties of the CFRP used are shown in Table 4.

5.1. Horizontal CFRP sheets on the side surfaces of top and bottom chords

In the present simulation, externally bonded horizontal CFRP sheets were applied on the side surfaces of top and bottom chords, with the width of the CFRP sheets being equal to the height of the top/bottom chord. The examined parameters in this part included the length and the thickness of the CFRP sheets. Three types of CFRP sheet length (650 mm, 850 mm which was the length obtained in Allam's study [22], and 1050 mm) and three types of CFRP sheet thickness (1 layer which was obtained in

Allam's study [22], 2 layers and 3 layers) were chosen to investigate the effect of the length and the thickness of the CFRP sheets on the effectiveness of this strengthening scheme, respectively. The predicted load-deflection curves are shown in Fig. 13, and the predicted load-carrying capacities are shown in Table 7, in which the test result of the beam with an un-strengthened web opening (B2) is also shown for reference. As can be seen from Fig. 13 and Table 7, with this strengthening scheme adopted, both the strength and stiffness of the beam are enhanced significantly; and with the increase in either the length or the layers of the CFRP sheets, the loading capacity of the beam increases slightly: an increase in the length of CFRP sheets from 650 mm to 1050 mm leads to an increase in the loading capacity of 5.13%, and an increase in the layers of CFRP sheets from 1 to 3 leads to and an increase in the loading capacity of 3.82%. It can be seen from Figs. 11(g) and (h) that the failures of the two beams with an FRP-strengthened web opening tested by Allam [22] (B8 and B9) were dominated by the two main diagonal cracks which initiated at the opening corners closest to the loading point and the left support, respectively. Externally bonded horizontal CFRP sheets on the side surfaces of top and bottom chords can help to postpone the development of these two diagonal cracks and cracks in the chords, and therefore improve the load-carrying capacity of the beam.

5.2. Vertical side-bonded CFRP sheets/CFRP U-jackets/CFRP wraps on the two sides of the opening

In this simulation, one-layer vertical side-bonded CFRP sheets/CFRP U-jackets/CFRP wraps were applied on the two sides of the opening, with their width being 200 mm (equal to the width obtained in Allam's study [22]), in order to study the effectiveness of these three different strengthening schemes. The predicted load-deflection curves are shown in Fig. 14, and the predicted load-carrying capacities are shown in Table 7.

As can be seen from Fig. 14 and Table 7, with any one of these three strengthening schemes adopted, both the strength and stiffness of the beam are enhanced significantly. Vertical side-bonded CFRP sheets, CFRP U-jackets and CFRP complete wraps lead to an increase in the loading capacity of the beam by 19.24%, 28.29% and 39.81%, respectively, indicating that within these three strengthening schemes, the CFRP complete wraps are most effective in enhancing the capacity of the beam. Externally bonded vertical CFRP sheets on the two sides of the opening can postpone the development of the two main diagonal cracks initiated at the opening corners (Figs. 11g and h); and with the vertical deformations of the two ends of the CFRP sheets being restricted [CFRP complete wraps or CFRP U-jackets whose ends are connected with the floor slab using anchors if CFRP wraps cannot be applied (e.g., for the strengthening of T-section beams)], the premature debonding of the FRP sheets can be prevented, and thus the load-carrying capacity of the beam can be improved more effectively.

Moreover, for the CFRP wraps applied on the two sides of the opening, three types of width (100 mm, 200 mm which was the width obtained in Allam's study [22], and 300 mm) and three thicknesses (1 layer, 2 layers and 3 layers) were chosen to investigate the effect of the width and the layers on the effectiveness of the CFRP wraps. The predicted load-deflection curves are shown in Fig. 15, and the predicted load-carrying capacities are shown in Table 7. As can be seen from Fig. 15 and Table 7, in the studied case, the width and the thickness of CFRP wraps have no effect on the strength and stiffness of the beam, which implies that one-layer CFRP wraps with 100 mm in width is sufficient when this strengthening scheme is adopted.

5.3. Vertical side bonded CFRP sheets/CFRP U-jackets/CFRP wraps on the top and bottom chords

In the present simulation, one-layer vertical side bonded CFRP sheets/CFRP U-jackets/CFRP wraps were applied on the top and bottom chords, with their width being 450 mm (i.e., equal to the length of the chords), in order to study the effectiveness of these three different strengthening schemes. The predicted load-deflection curves are shown in Fig. 16, and the predicted load-carrying capacities are shown in Table 7. As can be seen from Fig. 16 and Table 7, the vertical side bonded CFRP sheets on the chords can only slightly enhance the strength of the beam; while the CFRP U-jackets and CFRP wraps on the chords can significantly enhance the strength of the beam, with the enhancement by the CFRP wraps being slightly larger. The development of the main diagonal cracks which initiate at the opening corners will extend to the top and bottom chords. The CFRP wraps/U-jackets applied on the chords can effectively restrict the development of such cracks and thus enhance the strength of the beam. However, the effectiveness in enhancing the strength of the beam by using CFRP wraps on the chords is much smaller than that by using CFRP wraps on the two sides of the opening (see Table 7), as the latter can more effectively restrict the development of the main diagonal cracks at the opening corners.

Furthermore, for the CFRP wraps on the top and bottom chords, three thicknesses (1 layer, 2 layers and 3 layers) were chosen to investigate the effect of the thickness on the effectiveness of the CFRP wraps. The predicted load-deflection curves are shown in Fig. 17, and the predicted load-carrying capacities are shown in Table 7. As can be seen from Fig. 17 and Table 7, in the studied case, the thickness of CFRP wraps has no effect on the strength and stiffness of the beam, which implies that one-layer CFRP wraps is sufficient when this strengthening scheme is adopted.

5.4. Combination of the strengthening schemes

It has been found from the above analyses that externally bonded horizontal CFRP sheets on the side surfaces of top and bottom chords (referred to as Strengthening scheme I), vertical CFRP wraps on the two sides of the opening (referred to as Strengthening scheme II) and vertical CFRP wraps on the top and bottom chords (referred to as Strengthening scheme III) can effectively enhance the strength and stiffness of the beam. Therefore, it can be inferred that the combination of these three strengthening schemes may be the best way to strengthen the weakened beam by the creation of a web opening. In this part, four combining strengthening schemes were examined: (1) Combining strengthening scheme I: the combination of Strengthening scheme II and Strengthening scheme III ; (2) Combining strengthening scheme II: the combination of Strengthening scheme I and Strengthening scheme II); (3) Combining strengthening scheme III: the combination of Strengthening scheme I and Strengthening scheme III; and (4) Combining strengthening scheme IV: the combination of Strengthening scheme I, Strengthening scheme II and Strengthening scheme III. In these four combining strengthening schemes, the length of the horizontal CFRP sheets on the side surfaces of top and bottom chords (Strengthening scheme I) is 650 mm, and the widths of vertical CFRP wraps on the two sides of the opening (Strengthening scheme II) and vertical CFRP wraps on the top and bottom chords (Strengthening scheme III) are respectively 100 mm and 450 mm. The predicted load-deflection curves are shown in Fig. 18, and the predicted load-carrying capacities are shown in Table 7. The predicted load-deflection curves from the three individual strengthening schemes are also shown in Fig. 18 for comparison purposes. As can be seen from Fig. 18 and Table 7, the combination of Strengthening scheme III with Strengthening scheme I (i.e. Combining strengthening scheme III) only further improves the load-carrying capacity of the beam very slightly compared with these two individual strengthening schemes, which implies that the strengthening effects of Strengthening scheme I and Strengthening scheme III for the beam are quite similar; as the function of both of these two individual strengthening schemes is mainly to restrict the development of cracks in the chords, complementary effect cannot be achieved by combining these two strengthening schemes. The combination of Strengthening scheme II with either Strengthening scheme I (i.e. Combining strengthening scheme II) or Strengthening scheme III (i.e. Combining strengthening scheme I) can effectively enhance the load-carrying capacity of the beam, which implies that the strengthening effects of Strengthening scheme II and Strengthening scheme I/III for the beam are complementary; the development of diagonal cracks near the corners of the opening can be effectively restrained by using Strengthening scheme II, while the development of cracks in the chords can be effectively restrained by using Strengthening scheme I/III. In addition, the combination of these three individual strengthening schemes (i.e. Combining strengthening scheme IV) only achieves a little higher enhancement of the load-carrying capacity of the beam than

Combining strengthening scheme I, which is due to the similar strengthening effects of Strengthening scheme I and Strengthening scheme III for the beam, as analyzed above. Therefore, the combination of Strengthening scheme II and Strengthening scheme I/III is a more economical option for the strengthening system. Compared with horizontal CFRP sheets on the side surfaces of top and bottom chords (Strengthening scheme I), vertical CFRP wraps on the top and bottom chords (Strengthening scheme III) confine the concrete in the chords, thus improving the ductility and strength of the chords. Therefore, Combining strengthening scheme I is recommended for the strengthening of RC beams with a web opening. The increment of the load-carrying capacity of the beam by using Combining strengthening scheme I is nearly 51%, which is much larger than that of the strengthening schemes adopted by Allam [22] (14% and 40% for B8 and B9 respectively). This further verifies the effectiveness of the recommended strengthening system.

6. CONCLUDING REMARKS

This paper has presented a study on the numerical simulation of RC beams with an FRP-strengthened rectangular opening. Utilizing the explicit dynamic analysis approach available in ABAQUS [19], a total of three FE approaches have been proposed and examined. For the simulation of concrete, both the initial elastic modulus of concrete given by ACI-318 [35] and the secant modulus of concrete as recommended by Ye [34] and Pimanmas [16] were examined for comparison purposes. On the basis of the results presented in the present paper, the following conclusions can be drawn:

1) The adopted dynamic analysis approach with the key elements being properly determined can be used to simulate the static structural response of RC beams with an FRP-strengthened rectangular opening. The brittle cracking model with the secant modulus of concrete, which can provide the best predictions of load-deflection curves of existing test beams, is recommended for use in such simulation;
2) The brittle cracking model with the initial modulus of concrete consistently overestimates the ultimate loads and the stiffness of the test beams, while the concrete damaged plasticity model usually underestimates the ultimate loads and overestimates the stiffness of the test beams; and
3) By using the recommended FE approach (i.e. the brittle cracking model with the secant modulus of concrete), parametric studies were conducted. The results show that an FRP-strengthening system which combines the installation of vertical CFRP wraps on both the top and bottom chords and the two sides of the opening is recommended for use in the practice. The dimension and amount of the FRP used can be determined by using the recommended FE approach on the basis of the practical situation.

7. ACKNOWLEDGEMENT

The authors are grateful for the financial support received from the National Natural Science Foundation of China (Project No. 51878310) and the Research Grants Council of the Hong Kong Special Administrative Region (Project No.: PolyU 5273/11E). The authors are also grateful to Prof. Jin-Guang Teng at The Hong Kong Polytechnic University for his contributions to this work.

APPENDIX A. EQUATIONS OF THE CONSTITUTIVE MODELS OF CONCRETE AND BI-MATERIAL BOND-SLIP MODELS

The exponential tension-softening curve of concrete proposed by Hordijk [32] is:

$$\frac{\sigma_t}{f_t} = \left[1 + \left(3.0\frac{w}{w_0}\right)^3\right] e^{\left(-6.93\frac{w}{w_0}\right)} - 10\frac{w}{w_0} e^{(-6.93)} \tag{A1}$$

$$w_0 = 5.14\frac{G_F}{f_t} \tag{A2}$$

where σ_t (*MPa*) is the tensile stress normal to the crack direction; f_t (*MPa*) is the tensile strength of concrete; w (*mm*) and w_0 (*mm*) are respectively the crack opening displacement and the crack opening displacement at the complete release of stress or fracture energy; and G_F (*N/m*) is the required tensile fracture energy to create a stress-free crack over a unit area. In the present study, f_t and G_F were calculated using the equations from CEB-FIP [31], as shown in Eq. A3 and Eq. A4 respectively.

$$f_t = 1.4\left(\frac{f_c - 8}{10}\right)^{\frac{2}{3}} \tag{A3}$$

$$G_F = (0.0469D_a^2 - 0.5D_a + 26)\left(\frac{f_c}{10}\right)^{0.7} \tag{A4}$$

where f_c (*MPa*) is the cylinder compressive strength of concrete; and D_a (*mm*) is the maximum aggregate size, which is assumed to be 20 mm if there are no test data provided.

The Shear retention factor model of cracked concrete proposed by Rots [36] is:

$$\beta_s = \left(1 - \frac{\varepsilon_{cr}}{\varepsilon_{cr,u}}\right)^n \tag{A5}$$

where ε_{cr} is the concrete cracking strain; $\varepsilon_{cr,u}$ is the concrete cracking strain when the stress or fracture energy completely releases, which can be obtained from w_0 on the basis of the crack band concept (see Ref. [33] for details); and n is the exponent controlling the rate of shear degradation, which was chosen to be 5 following Nie's study [20]. A parametric study with different values of *n* (2, 3, 4, 5 and 6) considered was conducted by Nie [20]. It was found from the analysis that the exponent *n* of 5 led to the most accurate prediction of the load-deflection curve than other values (the values of 2, 3 or 4 overestimated the load while the value of 6 underestimated the load).

The uniaxial compressive stress-strain curve of concrete proposed by Saenz [37] is:

$$\sigma = \frac{\alpha\varepsilon}{1+[(\alpha\varepsilon_p / \sigma_p)-2](\varepsilon / \varepsilon_p)+(\varepsilon / \varepsilon_p)^2} \tag{A6}$$

where σ and ε are the compressive stress and the compressive strain respectively; σ_p and ε_p are the maximum stress and the corresponding strain respectively, which are assumed to be the cylinder compressive strength of concrete (f_c) and 0.002 respectively following Ref. [38] if no test data are provided; and α is the coefficient representing the initial tangent modulus of the concrete and is set to be equal to the elastic modulus of the concrete E_0 ($E_0 = 4730\sqrt{f_c}$ according to ACI-318 [35], where both E_0 and f_c are in *MPa*).

The stiffness degradation variable of cracked concrete (d_t) is:

$$d_t = 1-\beta_s \tag{A7}$$

where β_s is the shear retention factor defined by Eq. A5. For the concrete damaged plasticity model, the exponent *n* in Eq. A5 was chosen to be 5 following Chen et al.'s study [29].

The bond-slip model of CEB-FIP [31] is :

$$\tau^s = \begin{cases} \tau^s_{\max}\left(\dfrac{s}{s_1}\right)^{\varphi} & for \quad s \le s_1 \\ \tau^s_{\max} & for \quad s_1 < s \le s_2 \\ \tau^s_{\max} - (\tau^s_{\max} - \tau^s_f)\dfrac{s - s_2}{s_3 - s_2} & for \quad s_2 < s \le s_3 \\ \tau^s_f & for \quad s > s_3 \end{cases} \tag{A8}$$

where τ^s (MPa) is the local shear bond stress; s (mm) is the slip; $s_1 = s_2 = 0.6$ mm and $s_3 = 1.0$ mm for deformed steel bars; $s_1 = s_2 = s_3 = 0.1$ mm for plain steel bars; φ = 0.4 and 0.5 respectively for deformed steel bars and plain steel bars; $\tau^s_{\max} = 2\sqrt{f_c}$ (MPa) and $\tau^s_f = 0.5\tau^s_{max}$ (MPa) for deformed steel bars; and $\tau^s_f = \tau^s_{max} = 0.3\sqrt{f_c}$ (MPa) for plain steel bars.

The bond-slip model for externally bonded FRP reinforcement proposed by Lu et al. [39] is:

$$\tau = \begin{cases} \tau_{\max}\sqrt{\dfrac{s}{s_0}} & for \quad s \le s_0 \\ \tau_{\max} e^{-\alpha\left(\frac{s}{s_0}-1\right)} & for \quad s > s_0 \end{cases} \tag{A9}$$

$$s_0 = 0.0195\beta_{\mathrm{w}} f_t \tag{A10}$$

$$\tau_{\max} = \alpha_1 \beta_{\mathrm{w}} f_t \tag{A11}$$

$$\beta_{\mathrm{w}} = \sqrt{\frac{2 - b_f / b_c}{1 + b_f / b_c}} \tag{A12}$$

$$f_t = 0.395(f_{cu})^{0.55} \tag{A13}$$

$$\alpha = \frac{1}{\frac{G_{\mathrm{f}}}{\tau_{\max} s_0} - \frac{2}{3}} \tag{A14}$$

$$G_f = 0.308\beta_w^2\sqrt{f_t} \tag{A15}$$

where τ (MPa) is the local shear bond stress; $\tau_{\max}$ (MPa) is the local bond strength; s (mm) is the slip; s_0 (mm) is the slip when the bond stress reaches $\tau_{\max}$; β_{w} is the width ratio factor; b_f (mm) is the width of FRP; b_c (mm) is the width of beam; f_{cu} (MPa) is the cube compressive strength of concrete; G_f is the interfacial fracture energy; and $\alpha_1 = 1.5$.

DATA AVAILABILITY

The raw/processed data required to reproduce these findings cannot be shared at this time as the data also forms part of an ongoing study.

REFERENCES

[1] Kennedy, J.B. and Abdalla, H. (1992). "Static response of prestressed girders with openings", *Journal of Structural Engineering*, ASCE, 118(2), 488-504.

[2] Mansur, M.A. (1998). "Effect of opening on the behaviour and strength of R/C beams in shear", *Cement and Concrete Composites*, 20(6), 477-486.

[3] Tan, K.H., Mansur, M.A., and Wei, W. (2001). "Design of reinforced concrete beams with circular openings", *ACI Structural Journal*, 98(3), 407-415.

[4] Mansur, M.A., Tan K.H. and Wei, W. (1999). “Effects of creating an opening in existing beams”, *ACI Structural Journal*, 96(6), 899-906.

[5] Maaddawy, T. and Sherif, S. (2009). “FRP composite for shear strengthening of reinforced concrete deep beams with openings”, *Composite Structures*, 89(1), 60-69.

[6] Maaddawy, T. and El-Ariss, B. (2012). “Behavior of concrete beams with short shear span and web opening strengthened in shear with CFRP composites”, *Journal of Composites for Construction*, ASCE, 16(1), 47-59.

[7] Teng, J.G., Chen, J.F., Smith S.T. and Lam L. (2002). *FRP-strengthened RC structures*, John Wiley and Sons Ltd, UK, 245pp.

[8] Chen, J.F. and Teng, J.G. (2003). “Shear capacity of FRP-strengthened RC beams: FRP debonding”, *Construction and Building Materials*, 17(1), 27-41.

[9] Chen, J.G. and Teng, J.G. (2003). “Shear capacity of fiber-reinforced polymer-strengthened reinforced concrete beams: Fiber reinforced polymer rupture”, *Journal of Structural Engineerin*g, ASCE, 129(5), 615-625.

[10] Naser, M., Hawileh, R., Abdalla, J.A. and Al-Tamimi, A. (2012). “Bond behavior of CFRP cured laminates: experimental and numerical investigation”, *Journal of Engineering Materials and Technology*, 134(2), 719-728.

[11] Hawileh, R.A., Naser, M.Z. and Abdalla, J.A. (2013). “Finite element simulation of reinforced concrete beams externally strengthened with short-length CFRP plates”, *Composites Part B-Engineering*, 45(1), 1722-1730.

[12] Zhang, S.S. and Teng, J.G. (2014). “Finite element analysis of end cover

separation in RC beams strengthened in flexure with FRP", *Engineering Structures*, 75, 550-560.

[13] Zhang, S.S. and Teng, J.G. (2016). "End cover separation in RC beams strengthened in flexure with bonded FRP reinforcement: simplified finite element approach", *Materials and Structures*, 49(6), 2223-2236.

[14] Choobbor, S.S., Hawileh, R.A., Abu-Obeidah, A. and Abdalla, J.A. (2019). "Performance of hybrid carbon and basalt FRP sheets in strengthening concrete beams in flexure", *Composite Structures*, 227, 111337.

[15] Hawileh, R.A., Musto, H.A. and Abdalla, J.A. (2019). "Finite element modeling of reinforced concrete beams externally strengthened in flexure with side-bonded FRP laminates", *Composites Part B-Engineering*, 173, 106952.

[16] Pimanmas, A. (2010). "Strengthening R/C beams with opening by externally installed FRP rods: behavior and analysis", *Composite Structures*, 92(8), 1957-1976.

[17] Chin, S.C., Shafiq, N. and Nuruddin, M.F. (2012). "Strengthening of RC beams with large openings in shear by CFRP laminates: experiment and 2D nonlinear finite element analysis", *Research Journal of Applied Sciences Engineering and Technology*, 4(9), 1172-1180.

[18] Hawileh, R., El-Maaddawy, T., and Naser, M. (2012). "Nonlinear finite element modeling of concrete deep beams with openings strengthened with externally-bonded composites", *Materials and Design*, 42, 378-387.

[19] ABAQUS (2012). *ABAQUS Analysis User's Manual (Version 6.12)*, Dassault

Systems SIMULIA Corporation, Providence, Rhode Island, USA.

[20] Nie, X.F. (2018). *Behavior and modelling of RC beams with an FRP-strengthened web opening*, Ph.D Thesis, The Hong Kong Polytechnic University. (http://ira.lib.polyu.edu.hk/handle/10397/80150).

[21] Abdalla, H.A., Torkey, A.M., Haggag, H.A. and Abu-Amira, A.F. (2003). "Design against cracking at openings in reinforced concrete beams strengthened with composite sheets", *Composite Structures*, 60(2), 197-204.

[22] Allam, S. M. (2005). "Strengthening of RC beams with large openings in the shear zone", *Alexandria Engineering Journal*, *44*(1), 59-78.

[23] Suresh, J. and Prabhavathy, R. A. (2015). "Behaviour of steel fibre reinforced concrete beams with duct openings strengthened by steel plates", *International Journal of Advanced Information in Arts, Science & Management*, 4(4).

[24] Chin, S.C., Shafiq, N. and Nuruddin, M.F. (2016). "Behaviour of RC beams with CFRP-strengthened openings", *Structural Concrete*, 17(1), 32-43.

[25] Teng, J.G., Zhang, S.S., Jing, D.H., Nie, X.F. and Chen, G.M. (2013). "Seismic retrofit of RC frames through beam-end weakening in conjunction with FRP strengthening", *Proceedings of the 4th Asia-Pacific Conference on FRP in Structures (APFIS 2013)*, 1-8.

[26] WCOMD (1998). *Users guide for WCOMD-SJ*, Concrete Engineering Laboratory, Department of Civil Engineering, University of Tokyo.

[27] Cervenka, V., Jendele, L. and Cervenka, J. (2010). *ATENA program documentation part 1- theory*, Cervenka Consulting Ltd., Prague.

[28] ANSYS (2007). *A finite element computer software and user manual for nonlinear structural analysis*, Canonsburg, PA: ANSYS 2007 Inc.

[29] Chen, G.M., Chen, J.F. and Teng, J.G. (2012). "On the finite element modelling of RC beams shear-strengthened with FRP", *Construction and Building Materials*, 32, 13-26.

[30] Bazant, Z.P. and Oh, B.H. (1983). "Crack band theory for fracture of concrete", *Materials and Structures*, 16(3), 155-177.

[31] CEB-FIP (1993). *CEB-FIP Model Code 90*, Thomas Telford, London.

[32] Hordijk, D.A. (1991). *Local approach to fatigue of concrete*, PhD thesis, Delft University of Technology.

[33] Chen, G.M., Teng, J.G. and Chen, J.F. (2011). "Finite element modeling of intermediate crack debonding in FRP-plated RC beams", *Journal of Composites for Construction*, ASCE, 15(3), 399-353.

[34] Ye, L.P. (2005). *Concrete Structures* (Second Edition), Tsinghua University Press, Beijing, China. (in Chinese)

[35] American Concrete Institute (ACI) (2019). *Building code requirements for structural concrete and commentary*, ACI 318-19, Farmington Hills, MI.

[36] Rots, J. G. (1988). *Computational modeling of concrete fracture*, Ph.D. thesis, Delft University of Technology.

[37] Saenz, L. P. (1964). "Discussion of 'Equation for the stress-strain curve of concrete' by P. Desayi and S. Krishan", *ACI Journal*, 61(9), 1229-1235.

[38] Chen, W. F. (1982). *Plasticity in reinforced concrete*, McGraw-Hill, New York.

[39] Lu, X.Z., Teng, J.G. Ye, L.P. and Jiang, J.J. (2005). "Bond-slip models for FRP sheets/plates bonded to concrete", *Engineering Structures*, 27(6), 920-937.

[40] Kotynia, R., Abdel Baky, H., Neale, K.W. and Ebead, U.A. (2008). "Flexural strengthening of RC beams with externally bonded CFRP systems: Test results and 3D nonlinear FE analysis", *Journal of Composites for Construction*, 12(2), 190-201.

[41] Chen, G.M., Teng, J.G., Chen, J.F. and Xiao, Q.G. (2015). "Finite element modeling of debonding failures in FRP-strengthened RC beams: a dynamic approach", *Computers and Structures*, 158, 167-183.

[42] Clough, R. W. and Penzien, J. (1995). *Dynamics of structures*, Computers & Structures, Inc.

[43] Xu, X.P. and Needleman, A. (1994). "Numerical simulations of fast crack growth in brittle solids", *Journal of the Mechanics and Physics of Solids*, 42(9), 1397-1434.

Table 1. Summary of experimental studies on RC beams with an FRP-strengthened web opening

Source	Beam dimensions			Parameters studied	Shape of web opening	Number of web openings	Web opening size (mm)	Load capacity reduction (%)[a]	Strengthening scheme	Increase in load capacity due to strengthening (%)[b]	Observed failure mode		Remarks
	Span (mm)	Width (mm)	Height (mm)								Without strengthening	With strengthening	
Mansur et al. [4]	2600	200[c]	500	W or w/o FRP-strengthening	Circular	2[d]	r=150	29.5	Bonded FRP plates	52.8	Shear crack passing through the opening	Flexural at mid-span	Reversed T-section beams with circular openings (the flange is 100 mm in height and 700 mm in width)
Abdalla et al. [21]	2000	100	250	Opening size and w or w/o FRP-strengthening	Rectangular	1	100 × 100[e]	50.6	Bonded FRP sheets and wraps	109.8	Shear crack passing through the opening corners	Flexural at mid-span	NA
							200 × 100	48.2		76.7		Shear at opening	
							300 × 100	50.6		51.2		Shear at opening	
							300 × 150	73.5		59.1		Shear at opening	
Allam [22]	3200	150	400	W or w/o FRP-strengthening	Rectangular	1	450 × 150	37.1	Bonded FRP sheets and U-jackets	14.3/40.0	Shear crack passing through the opening corners	Shear at opening after debonding of FRP	NA
Maaddawy and Sherif [5]	1000	80	500	Opening size, location and w or w/o FRP-strengthening	Rectangular	2	200 × 200	NA	Bonded FRP sheets and wraps	66.0	Shear crack passing through the opening corners, and shear crack in the chords	Shear at opening and chords after debonding of FRP	Deep beams, no control beam without opening was tested
							250 × 250	NA		65.3			
Pimanmas [16]	2100	400	160	Opening shape and w or w/o FRP-strengthening	Circular	2	r=150	37.7	Near-surface mounted FRP rods	57.6	Shear crack passing through the opening corners	Flexural at mid-span	NA
					Rectangular		150 × 150	44.3		75.4			
Chin et al. [17]	1800	300	120	Opening location and w or w/o FRP-strengthening	Rectangular	2	210 × 210	74.4	Bonded FRP sheets and wraps	80.1	Shear crack passing through the opening corners	Shear at opening	NA
							210 × 210	68.8		48.8			

Maaddawy and Ariss [6]	2400	85	400	Opening size and w or w/o FRP-strengthening	Rectangular	1	200 × 200	72.7	Bonded FRP sheets and U-jackets	276.2	Shear crack passing through the opening corners	Shear at opening and in chords after debonding and rupture of FRP	NA
							350 × 200	70.1		160.9			
							500 × 120	44.2		69.8	Shear crack passing through the opening corners, and shear crack in the chords		
							500 × 160	46.8		61.0			
							500 × 200	58.4		65.6			
Chin et al. [24]	1800	120	300	W or w/o FRP-strengthening	Rectangular	2	800 × 140	58.4	Bonded FRP sheets	95.6	Shear crack passing through the opening corners	Shear at opening after debonding of FRP	NA
Teng et al. [25]	3300	250(c)	500	NA	Rectangular	1	500 × 220	NA	Bonded FRP plate, U-jackets and wraps	NA	Shear crack passing through the opening corners	Shear at opening	Reversed T- section beams whose flange is 100 mm in height and 1450 mm in width

Note: (a) Compared with control beam specimen without a web opening; (b) Compared with beam specimen with an un-strengthened web opening; (c) Web width; (d) Symmetrically located in the two shear spans; (e) Opening width × opening height.

Table 2. Summary of numerical studies on RC beams with an FRP-strengthened web opening

Source	Software used	Modelling of concrete cracking			Modelling of bond behaviour	
		Crack modelling method	Tension-softening behavior	Shear stress transfer model	Steel-to-concrete	FRP-to-concrete
Pimanmas [16]	WCOMD	Smeared crack model	$\sigma_t = f_t(\frac{\varepsilon_{cr}}{\varepsilon_t})^{0.4}$	$\tau_{cr} = 3.8(f_c)^{1/3}\frac{\delta^2}{1+\delta^2}$	Perfect bond	Perfect bond
Chin et al. [17]	ATENA	Rotated crack model in the smeared crack approach	The slope of the ascending branch is equal to the concrete modulus of elasticity. In the descending branch of the stress-strain curve, a fictitious crack model based on a crack-opening law and fracture energy is used, where the cracks occur when the principal stress exceeds the tensile strength.	NA	Perfect bond	Bond-slip model developed by Lu et al. [39]
Hawileh et al. [18]	ANSYS ver. 11.0	Smeared crack model	σ_t increases linearly to f_t, then suddenly drops to $0.6f_t$, finally descends linearly to zero at a strain value of $6\varepsilon_{cr}$.	NA	Perfect bond	Bond-slip relationship proposed by Xu and Needleman [43]

Note : σ_t=tensile stress of concrete; ε_t=tensile strain of concrete; ε_{cr}=cracking strain of concrete; f_t= tensile strength of concrete; $\varepsilon_{cr}=2f_t/E_0$, where E_0 is the initial elastic modulus of concrete; f_c= cylinder compressive strength of concrete; τ_{cr}=shear stress of concrete; δ=normalized shear strain of concrete, defined as $\delta = \gamma_{cr}/\varepsilon_t$, where γ_{cr} is the shear strain of cracked concrete.

Table 3. Period of the fundamental vibration mode of simulated specimens

Source	Specimen	T_1 (s)
Maaddawy and Ariss [6]	S1-500×120	0.0117
	S2-500×120	0.0117
	S1-500×160	0.0119
	S2-500×160	0.0119
Abdalla et al. [21]	RO3	0.0109
	RO4	0.0110
Allam [22]	B8	0.0167
	B9	0.0167
Chin et al. [17]	B5	0.0103
	B6	0.00954
Chin et al. [24]	SBRO	0.00818
Teng et al. [25]	FRP-500×220	0.0153

Table 4. Collected RC test beams with an FRP-strengthened web opening for verification of the proposed FE approach

<table>
<tr><th rowspan="2">Source</th><th rowspan="2">Specimen</th><th rowspan="2">Shape of cross section</th><th colspan="3">Beam dimensions</th><th colspan="2">Opening size</th><th rowspan="2">Number of web opening</th><th colspan="2">FRP strengthening configuration</th><th rowspan="2">Observed failure mode</th></tr>
<tr><th>Span (mm)</th><th>Width (mm)</th><th>Height (mm)</th><th>Width (mm)</th><th>Height (mm)</th><th>Opening chords</th><th>Sides of opening</th></tr>
<tr><td rowspan="4">Maaddawy and Ariss [6]</td><td>S1-500×120</td><td rowspan="4">Rectangular</td><td rowspan="4">2400</td><td rowspan="4">85</td><td rowspan="4">400</td><td>500</td><td>120</td><td rowspan="4">1</td><td rowspan="2">One-layer horizontal CFRP sheet and one-layer vertical CFRP U-jacket/complete wrap</td><td rowspan="2">One-layer vertical CFRP U-jacket</td><td rowspan="4">Shear at opening</td></tr>
<tr><td>S1-500×160</td><td>500</td><td>160</td></tr>
<tr><td>S2-500×120</td><td>500</td><td>120</td><td rowspan="2">One-layer horizontal CFRP sheet and two-layer vertical CFRP U-jacket/complete wrap</td><td rowspan="2">Two-layer vertical CFRP U-jacket</td></tr>
<tr><td>S2-500×160</td><td>500</td><td>160</td></tr>
<tr><td rowspan="2">Abdalla et al. [21]</td><td>RO3</td><td rowspan="2">Rectangular</td><td rowspan="2">2000</td><td rowspan="2">100</td><td rowspan="2">250</td><td>200</td><td>100</td><td rowspan="2">1</td><td rowspan="2">One-layer horizontal CFRP sheet</td><td rowspan="2">One-layer CFRP wrapping</td><td rowspan="2">Shear at opening</td></tr>
<tr><td>RO4</td><td>300</td><td>100</td></tr>
<tr><td rowspan="2">Allam [22]</td><td>B8</td><td rowspan="2">Rectangular</td><td rowspan="2">3000</td><td rowspan="2">150</td><td rowspan="2">400</td><td>450</td><td>150</td><td rowspan="2">1</td><td>One-layer horizontal CFRP sheet</td><td>One-layer vertical CFRP sheet</td><td rowspan="2">Shear at opening</td></tr>
<tr><td>B9</td><td>450</td><td>150</td><td>One-layer vertical CFRP U-jacket and one-layer horizontal CFRP sheet</td><td>One-layer horizontal CFRP U-jacket and one-layer vertical CFRP sheet</td></tr>
<tr><td rowspan="2">Chin et al. [17]</td><td>B5</td><td rowspan="2">Rectangular</td><td rowspan="2">1800</td><td rowspan="2">120</td><td rowspan="2">300</td><td>210</td><td>210</td><td rowspan="2">2</td><td rowspan="2">One-layer horizontal CFRP plate</td><td rowspan="2">One-layer vertical CFRP plate</td><td rowspan="2">Shear at opening</td></tr>
<tr><td>B6</td><td>210</td><td>210</td></tr>
<tr><td>Chin et al. [24]</td><td>SBRO</td><td>Rectangular</td><td>1800</td><td>120</td><td>300</td><td>800</td><td>140</td><td>1</td><td>One-layer horizontal CFRP plate</td><td>NA</td><td>Shear at opening</td></tr>
<tr><td>Teng et al. [25]</td><td>FRP-500×220</td><td>T-section</td><td>3300</td><td>250^(a)</td><td>500</td><td>500</td><td>220</td><td>1</td><td>One-layer vertical CFRP wrap and one-layer horizontal CFRP plate</td><td>Two-layer vertical CFRP U-jacket</td><td>Shear at opening</td></tr>
</table>

Note: (a) Web width (Specimen FRP-500×220 is a reversed T-section beam whose flange is 100 mm in height and 1450 mm in width).

Table 5. Material properties of collected RC test beams with an FRP-strengthened web opening

Source	Specimen	Cylinder compressive strength of concrete f_c (MPa)	Steel reinforcement							FRP reinforcement		
			Tension steel bars	Yield strength of tension bars f_{yt} (MPa)	Compression steel bars	Yield strength of compression bars f_{yc} (MPa)	Stirrups	Yield strength of stirrups f_{vy} (MPa)	Elastic modulus of all steel bars E_s [(a)] (GPa)	Nominal thickness (mm)	Tensile strength (MPa)	Elastic modulus (GPa)
Maaddawy and Ariss [6]	S1-500×120	20	4Φ16 (deformed, and placed in two rows)	520	2Φ12 (deformed)	520	Φ6@80 (plain)	300	200	0.381	3450	230
	S2-500×120											
	S1-500×160											
	S2-500×160											
Abdalla et al. [21]	RO3	39.2	4Φ10 (deformed, and placed in two rows)	400	2Φ10 (deformed)	400	Φ8@150 (deformed)	240	200	0.13	3500	230
	RO4	40.8										
Allam [22]	B8	28	3Φ16 (deformed)	400	2Φ12 (deformed)	380	Φ8@150 (plain)	250	200	0.13	3500	230
	B9											
Chin et al. [17]	B5	35	2Φ12 (deformed)	410	2Φ10 (deformed)	410	Φ6@300 (plain)	275	200	1.4	2200	170
	B6											
Chin et al. [24]	SBRO	29.75	2Φ12 (deformed)	460	2Φ10 (deformed)	460	Φ6@300 (plain)	275	200	1.4	2200	170
Teng et al. [25]	FRP-500×220	33.2	4Φ20 (deformed)	482	3Φ20 (deformed)	482	Φ8@100 (plain)	375	200	0.337 (sheet) 1.2 (plate)	2738 (sheet) 2450 (plate)	238 (sheet) 131 (plate)

Note: (a) E_s is assumed to be 200 GPa as test data are not available in the relevant publications.

Table 6. Test and predicted ultimate loads

Source	Specimen	Test result (kN)	BC model with SECANT modulus (kN)		BC model with INITIAL modulus (kN)		DP model (kN)	
			Prediction	Prediction / test	Prediction	Prediction / test	Prediction	Prediction / test
Maaddawy and Ariss [6]	S1-500×120	72	74.2	1.03	90.6	1.26	44.4	0.617
	S2-500×120	73	75.7	1.04	104.6	1.45	45.6	0.624
	S1-500×160	57	62.7	1.09	87.0	1.53	32.5	0.571
	S2-500×160	66	64.0	0.970	75.8	1.15	33.5	0.507
Abdalla et al. [21]	RO3	73	72.2	0.989	78.3	1.07	77.3	1.06
	RO4	62	65.9	1.06	70.5	1.14	65.6	1.06
Allam [22]	B8	120	137.0	1.14	152.3	1.27	136.5	1.14
	B9	147	144.4	0.983	149.1	1.01	139.3	0.947
Chin et al. [17]	B5	36	32.1	0.891	36.6	1.02	33.6	0.934
	B6	37	30.5	0.825	36.6	0.989	32.4	0.875
Chin et al. [24]	SBRO	83	82.0	0.988	87.1	1.05	52.6	0.634
Teng et al. [25]	FRP-500×220	475	488.2	1.03	520.5	1.10	275.8	0.581
Statistical characteristics	**Average =**			1.00		1.17		0.796
	STD =			0.0848		0.175		0.228
	CoV =			0.0845		0.150		0.287

Table 7. Design of the FRP-strengthening system for specimens tested by Allam [22]

Strengthening scheme	Dimension of the bonded FRP sheet	Layers of the bonded FRP sheet	Predicted load-carrying capacity (kN)	Increase in load capacity due to strengthening (%)[(b)]
None	-	-	105.0[(a)]	-
Horizontal CFRP sheets on the side surfaces of top and bottom chords	650 mm in length	1	130.7	24.48
	850 mm in length	1	133.5	27.14
		2	138.5	31.90
		3	138.6	32.00
	1050 mm in length	1	137.4	30.86
Vertical CFRP sheets on the two sides of the opening	200 mm in width	1	125.2	19.24
Vertical CFRP U-jackets on the two sides of the opening	200 mm in width	1	134.7	28.29
Vertical CFRP wraps on the two sides of the opening	100 mm in width	1	146.7	39.71
	200 mm in width	1	146.8	39.81
		2	146.9	39.90
		3	147.0	40.00
	300 mm in width	1	146.8	39.81
Vertical CFRP sheets on the two chords of the opening	450 mm in width[(c)]	1	106.8	1.71
Vertical CFRP U-jackets on the two chords of the opening	450 mm in width	1	133.4	27.05
Vertical CFRP wraps on the two chords of the opening	450 mm in width	1	136.1	29.62
		2	137.3	30.76
		3	137.4	30.86
Vertical CFRP wraps on the two chords and the two sides of the opening	450 mm in width for the wraps on the chords and 100 mm in width for the wraps on the two sides of the opening	1	158.5	50.95
Vertical CFRP wraps on the two sides of the opening + horizontal CFRP sheets on the two chords	100 mm in width for the wraps on the two sides of the opening, and 650 mm in length for the horizontal CFRP sheets on the two chords	1	155.6	48.19
Vertical CFRP wraps on the two chords + horizontal CFRP sheets on the two chords	450 mm in width for the wraps on the chords, and 650 mm in length for the horizontal CFRP sheets on the two chords	1	136.3	29.81
Vertical CFRP wraps on the two chords and the two sides of the opening + horizontal CFRP sheets on the two chords	450 mm in width for the wraps on the chords, 100 mm in width for the wraps on the two sides of the opening, and 650 mm in length for the horizontal CFRP sheets on the two chords	1	162.2	54.48

Note: (a) Obtained from the test; (b) Compared with the beam specimen with an un-strengthened web opening (B2); (c) Equal to the length of the chords.

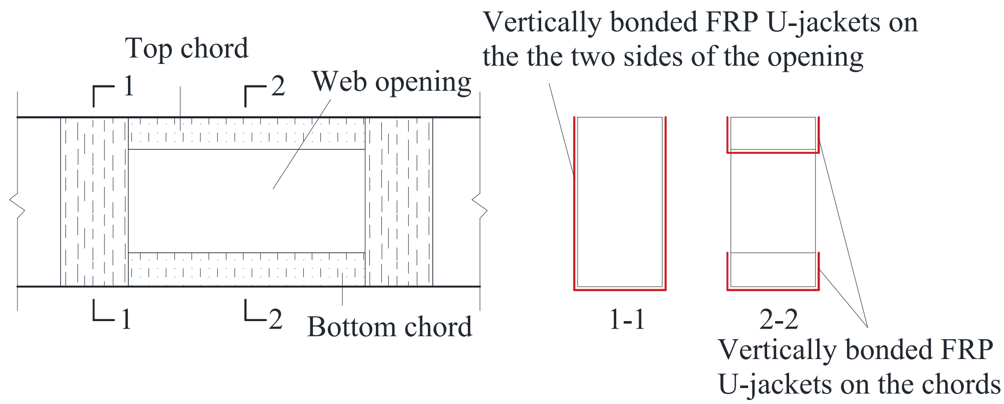
Top chord
Web opening
Vertically bonded FRP U-jackets on the the two sides of the opening
1
2
1
2
Bottom chord
1-1
2-2
Vertically bonded FRP U-jackets on the chords

(a)

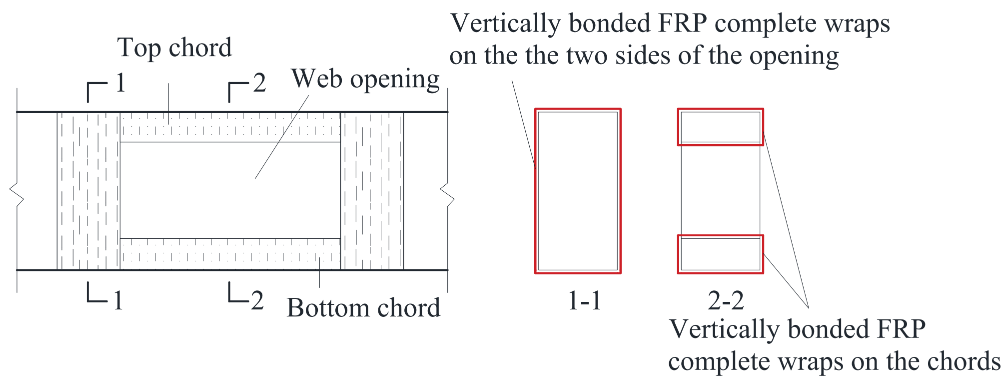
Top chord
Web opening
Vertically bonded FRP complete wraps on the the two sides of the opening
1
2
1
2
Bottom chord
1-1
2-2
Vertically bonded FRP complete wraps on the chords

(b)

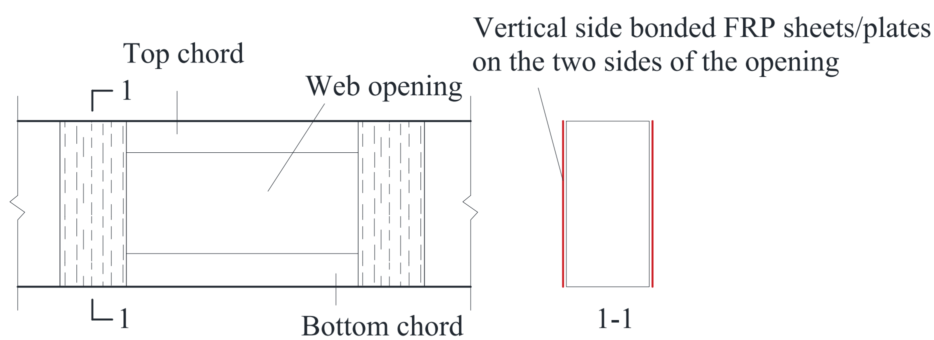
Top chord
Web opening
Vertical side bonded FRP sheets/plates on the two sides of the opening
1
1
Bottom chord
1-1

(c)

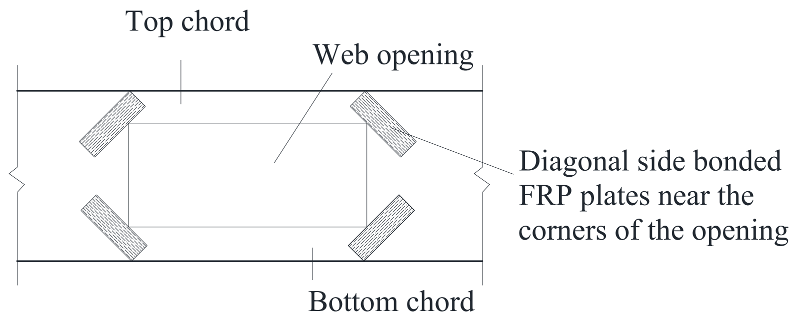

(d)

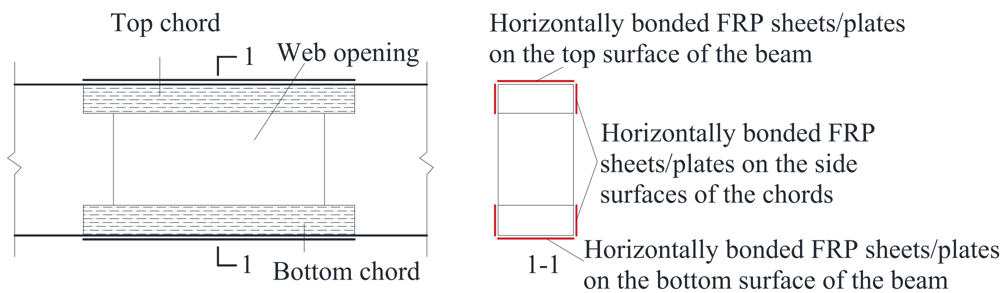

(e)

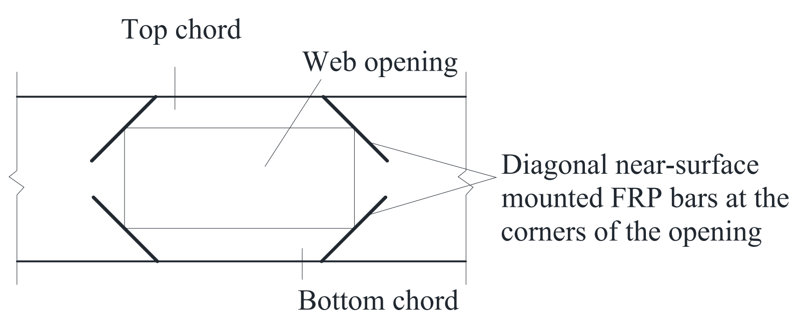

(f)

Figure 1. Diagrams of the main FRP-strengthening schemes proposed in existing experimental studies

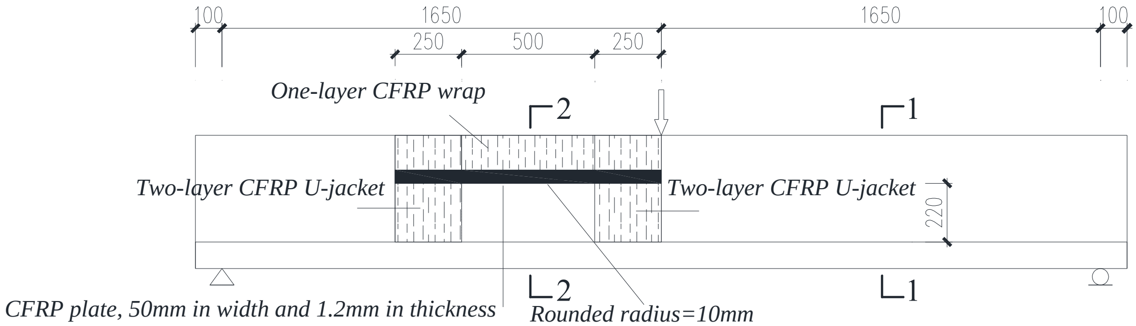

(a) Elevation

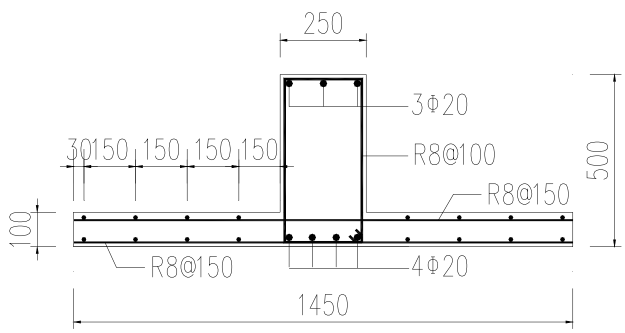

(b) Section 1-1

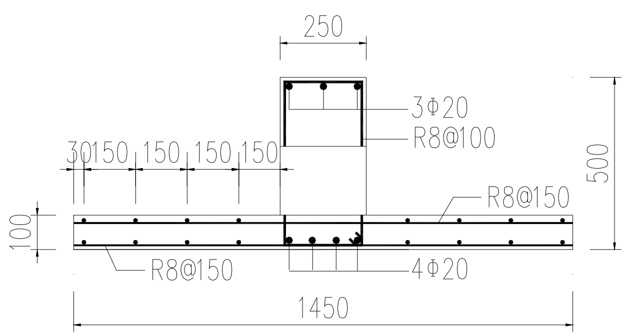

(c) Section 2-2

Figure 2. Details of the specimen tested by the authors' group (FRP-500×220) [25]
(Dimensions in mm)

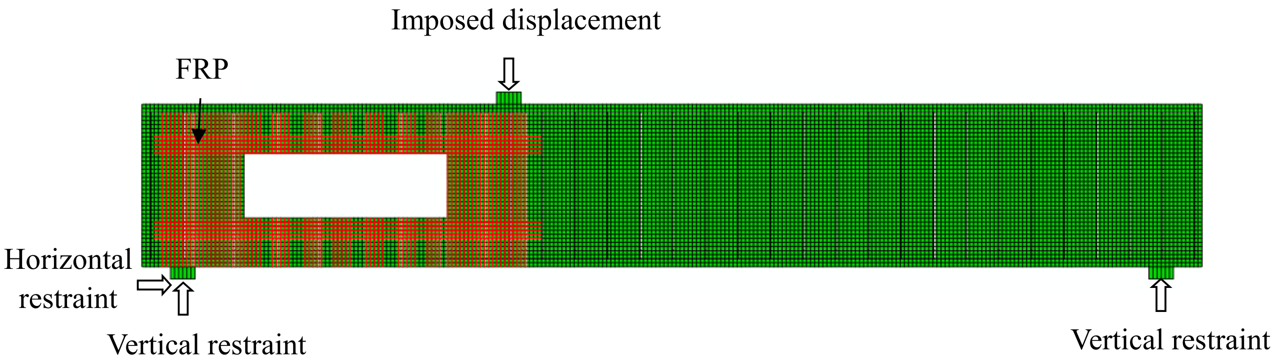

Figure 3. Typical FE meshes

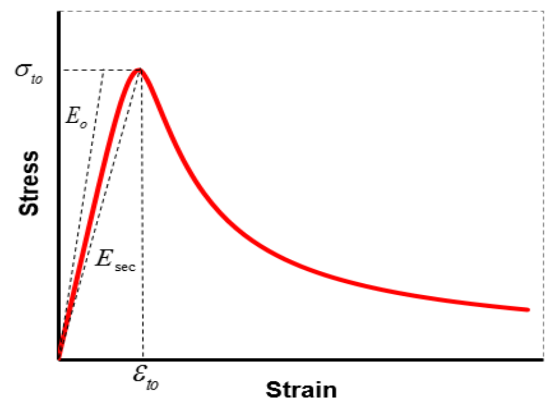

(Note: E_0=initial elastic modulus; E_{sec}=secant modulus)

Figure 4. Tensile stress-strain curve of concrete

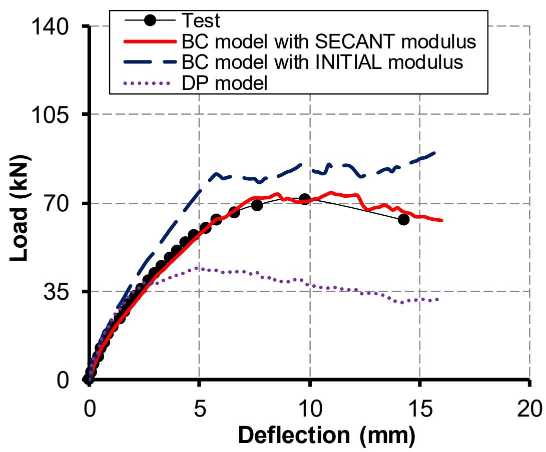

(a) S1-500×120 [6]

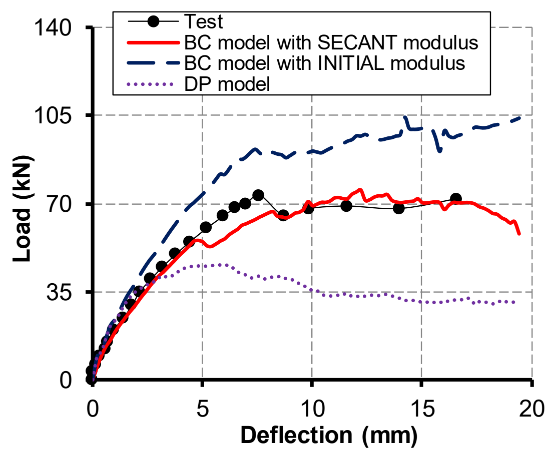

(b) S2-500×120 [6]

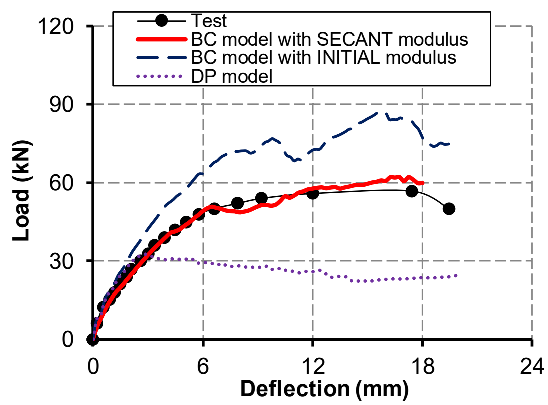

(c) S1-500×160 [6]

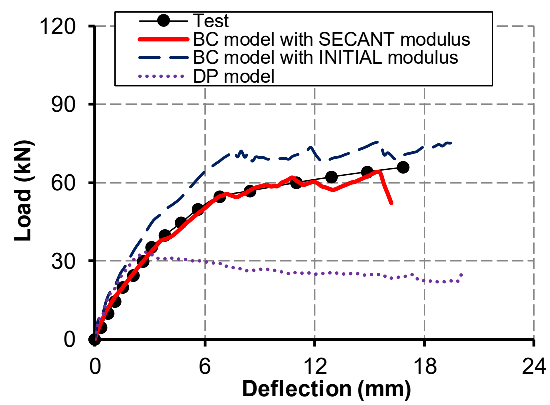

(d) S2-500×160 [6]

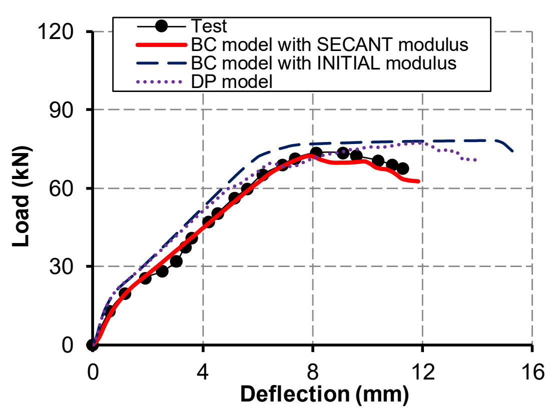

(e) RO3 (200×100) [21]

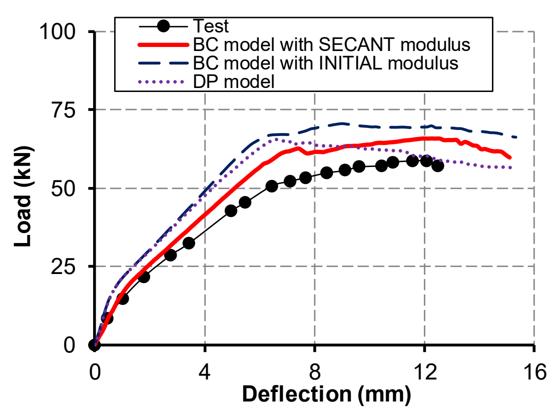

(f) RO4 (300×100) [21]

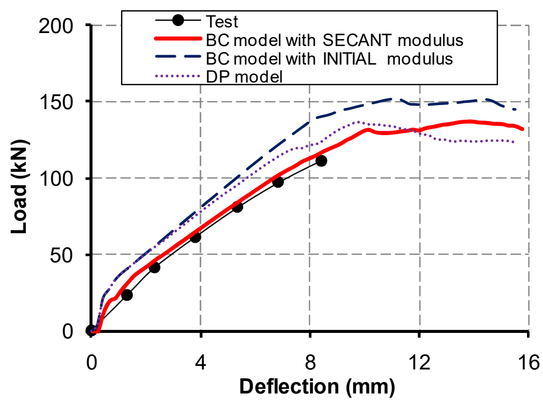

(g) B8 (450×150) [22]

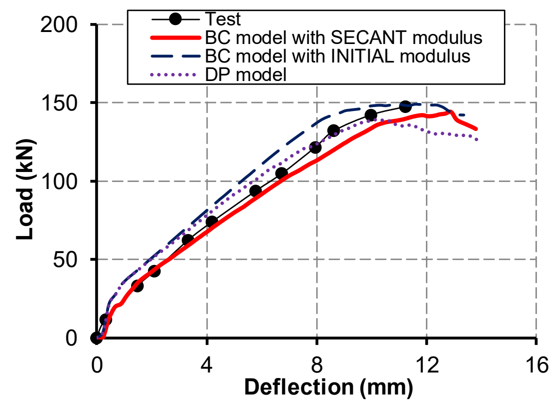

(h) B9 (450×150) [22]

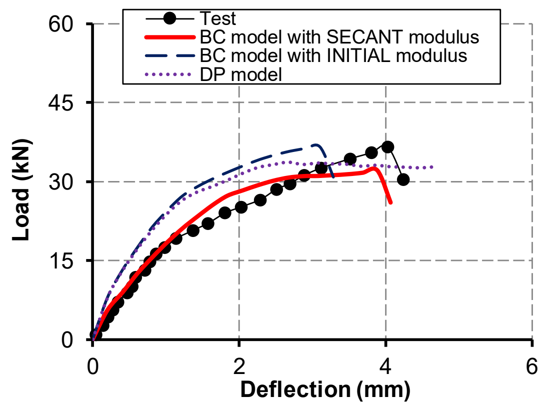

(i) B5 (210x210) [17]

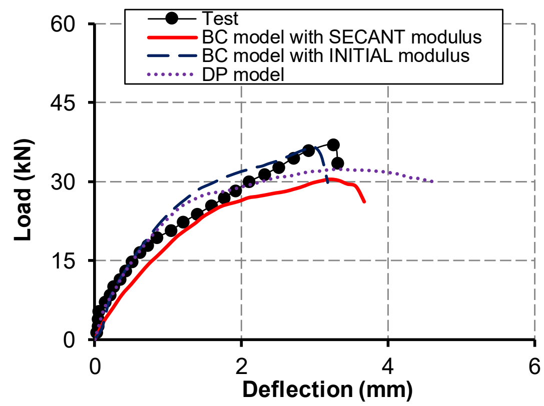

(j) B6 (210x210) [17]

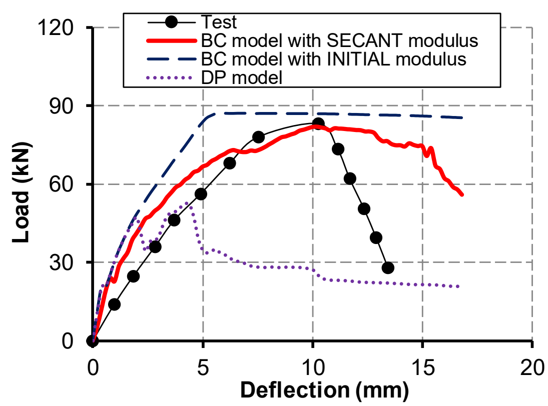

(k) SBRO (800x140) [24]

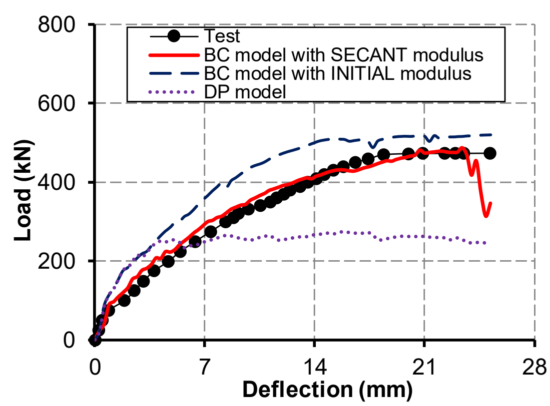

(l) FRP-500×220 [25]

Figure 5. Load-deflection curves

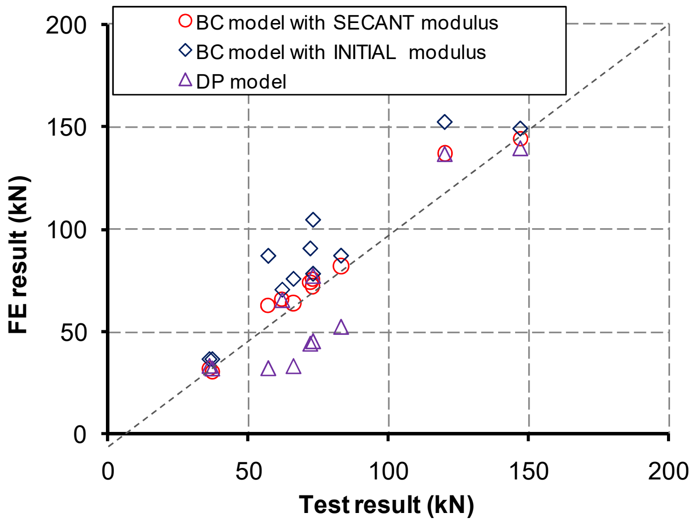

Figure 6. Comparison of ultimate loads between FE predictions and tests

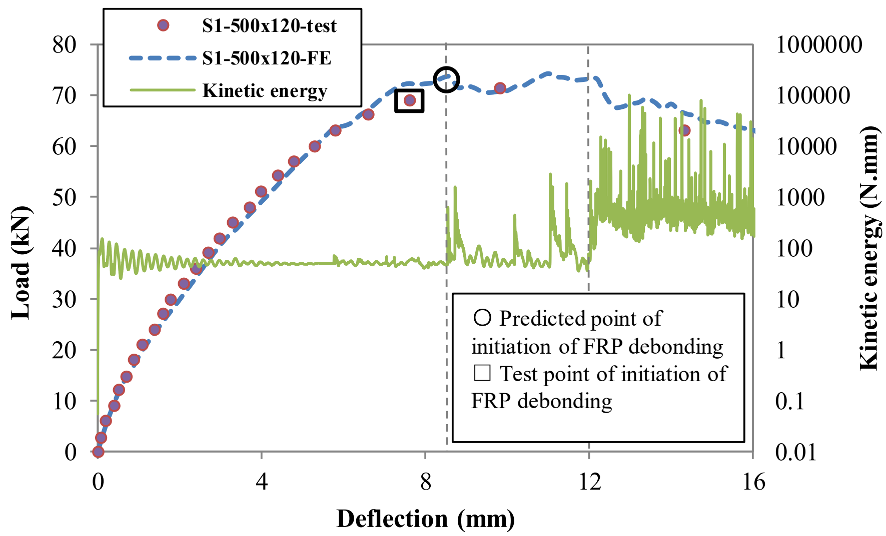

Figure 7. Development history of kinetic energy (S1-500×120)

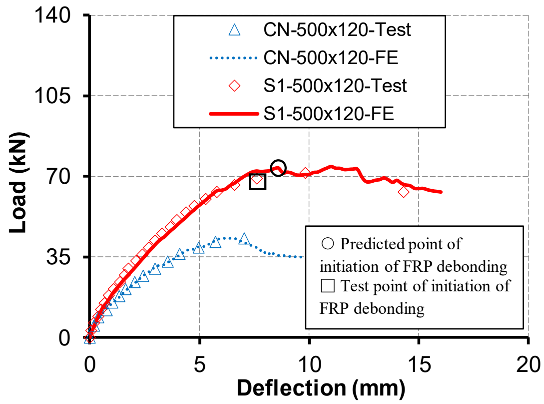

(a) S1-500×120 versus CN-500×120 [6]

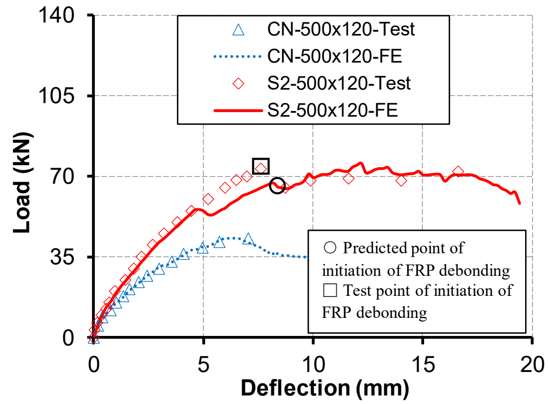

(b) S2-500×120 versus CN-500×120 [6]

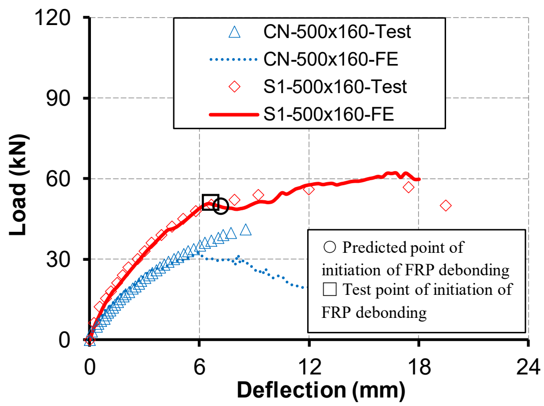

(c) S1-500×160 versus CN-500×160 [6]

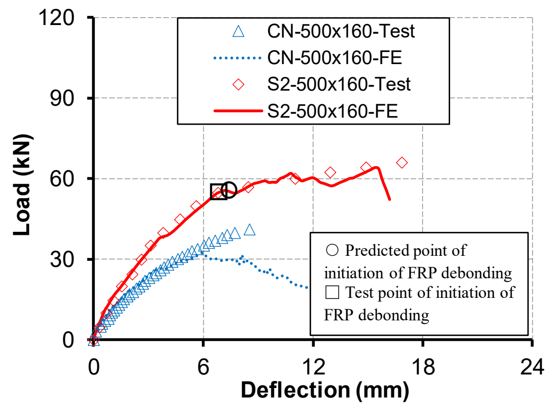

(d) S2-500×160 versus CN-500×120 [6]

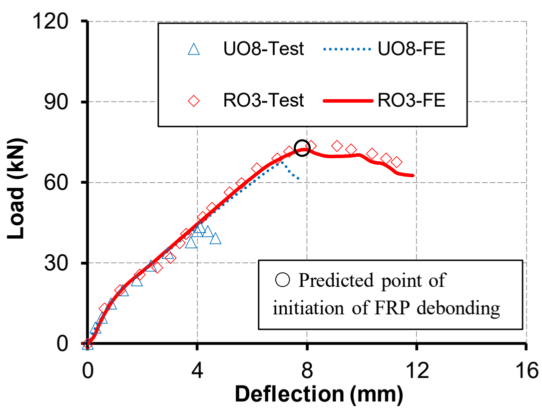

(e) RO3 versus UO8 (200×100) [21]

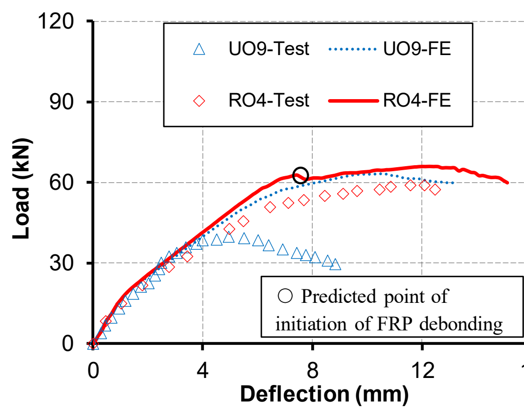

(f) RO4 versus UO9 (300×100) [21]

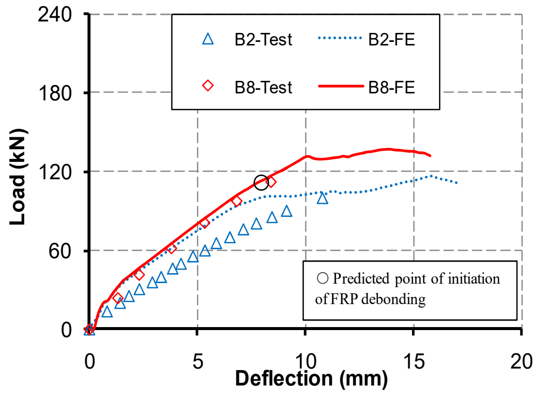

(g) B8 versus B2 (450×150) [22]

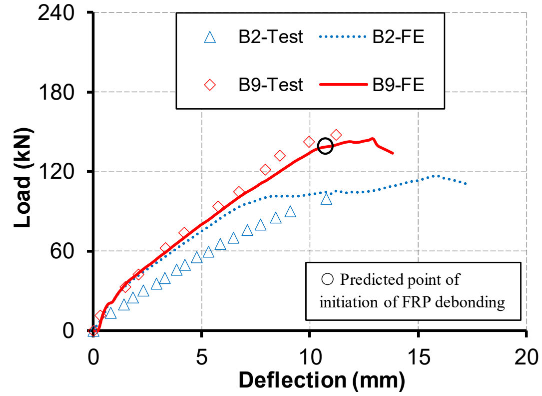

(h) B9 versus B2 (450×150) [22]

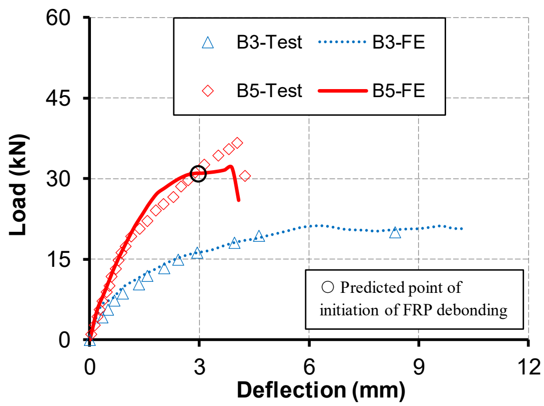

(i) B5 versus B3 (210x210) [17]

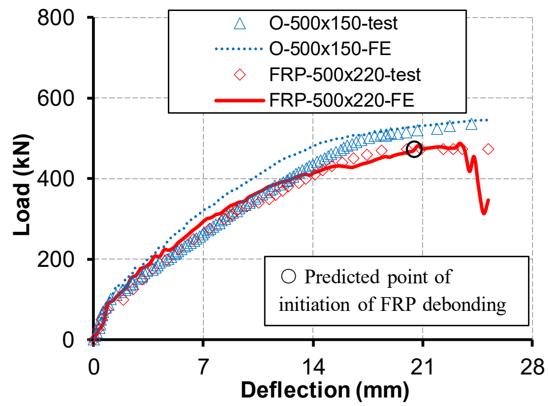

(j) FRP-500×220 versus O-500×150 [25]

Figure 8. Comparison between un-strengthened and FRP-strengthened beams

(a) FRP debonding at the opening corner nearest to the loading point

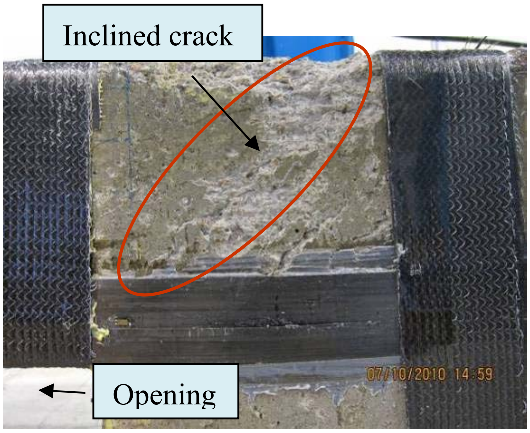

(b) Inclined crack at the opening corner nearest to the loading point

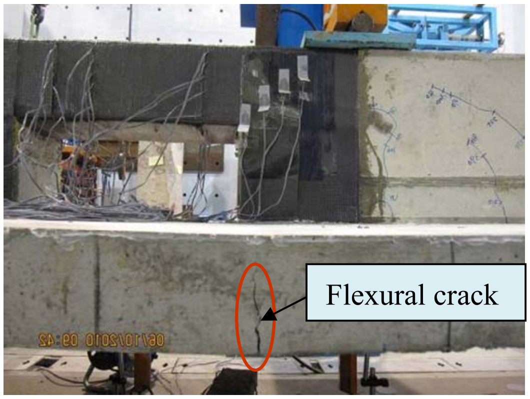

(c) Flexural crack at one end (closer to the loading point) of the flange chord near its bottom surface

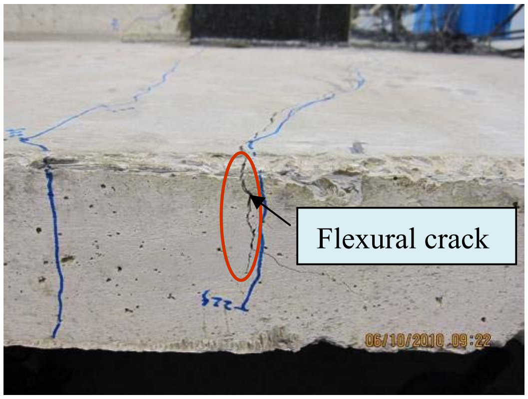

(d) Flexural crack at the other end (i.e., closer to the corresponding support) of the flange chord near its top surface

Figure 9. Failure mode of Specimen FRP-500×220 tested by the authors' group [25]

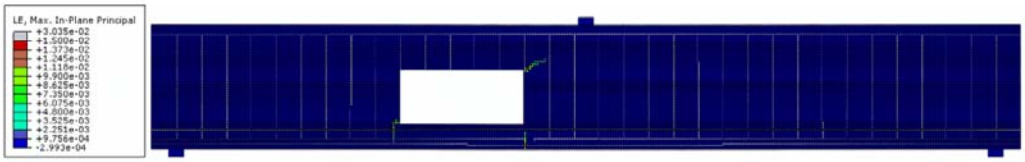

(a) 110 kN

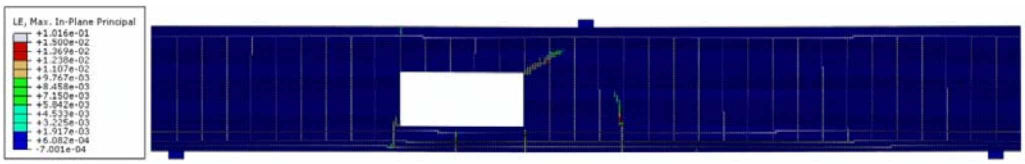

(b) 224 kN

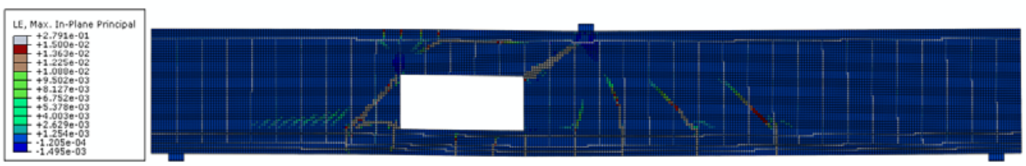

(c) 384 kN

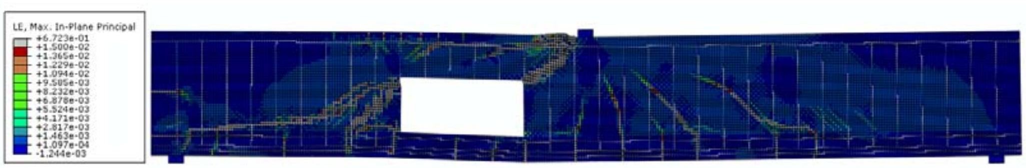

(d) 455 kN

Figure 10. Predicted failure process of Specimen FRP-500×220 tested by the authors' group [25]

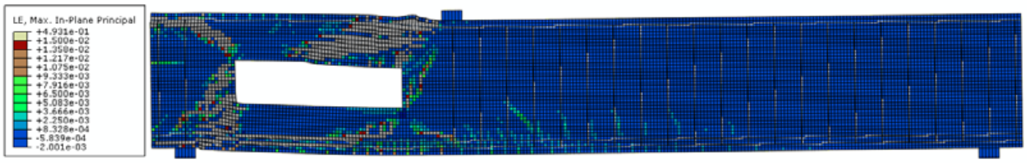

(a) S1-500×120 [6]

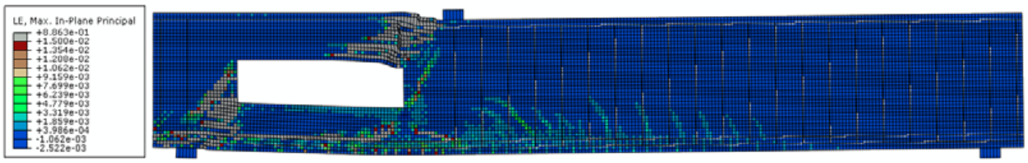

(b) S2-500×120 [6]

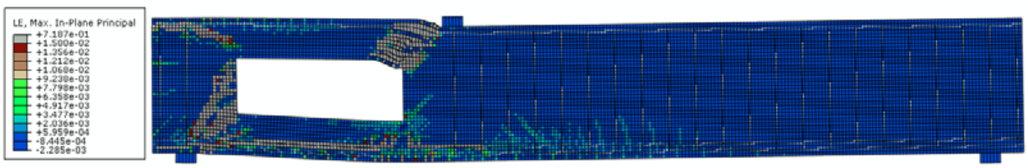

(c) S1-500×160 [6]

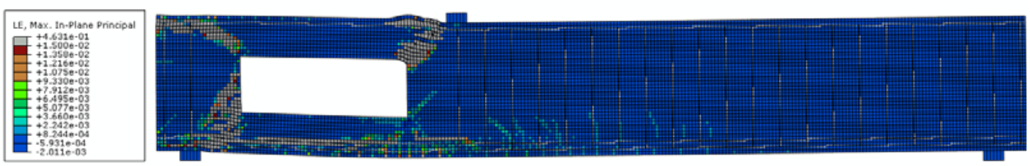

(d) S2-500×160 [6]

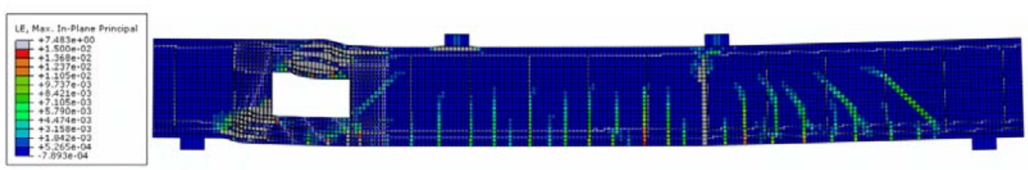

(e) RO3 (200×100) [21]

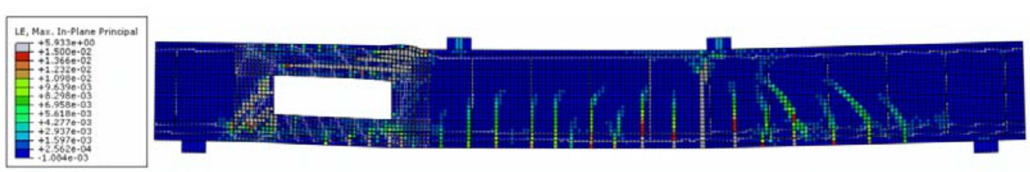

(f) RO4 (300×100) [21]

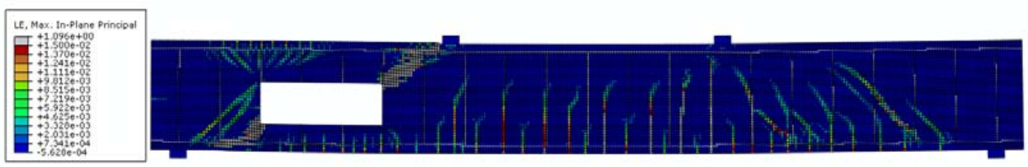

(g) B8 (450×150) [22]

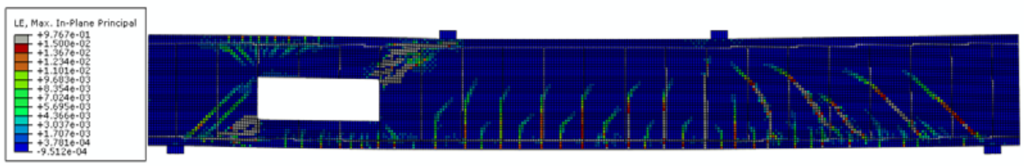

(h) B9 (450×150) [22]

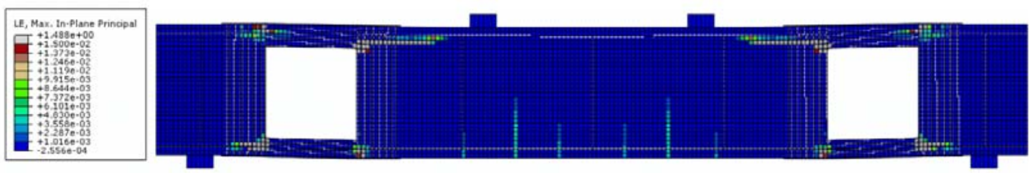

(i) B5 (210×210) [17]

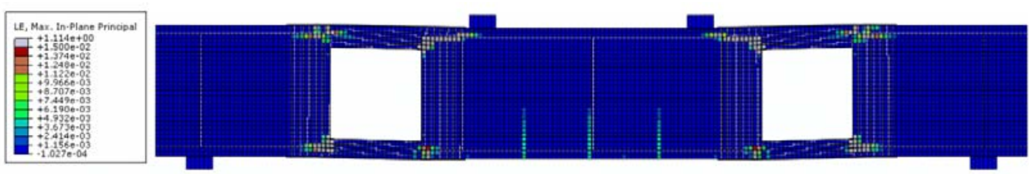

(j) B6 (210×210) [17]

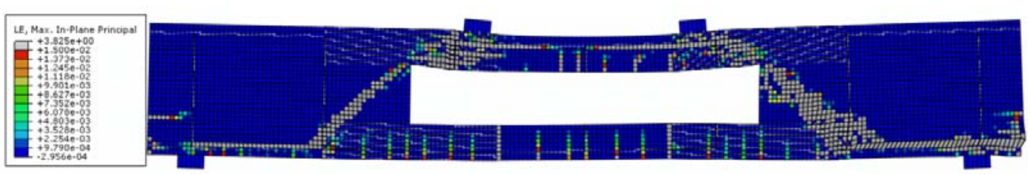

(k) SBRO (800×140) [24]

Figure 11. Predicted crack patterns at failure

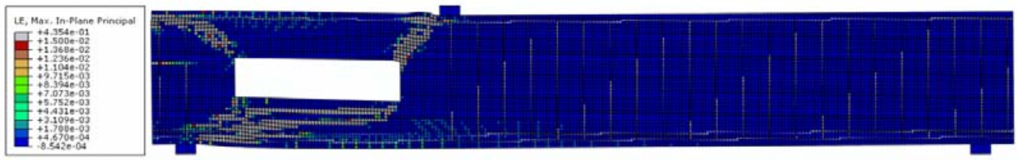

(a) CN-500×120

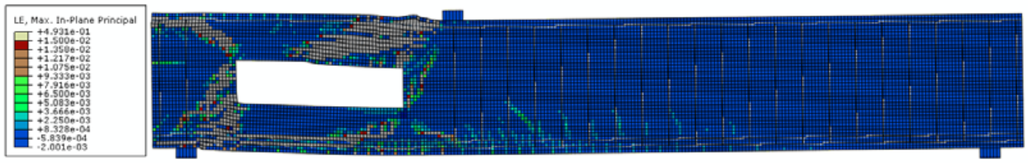

(b) S1-500×120

Figure 12. Comparison of predicted crack patterns at failure between un-strengthened and FRP-strengthened beams

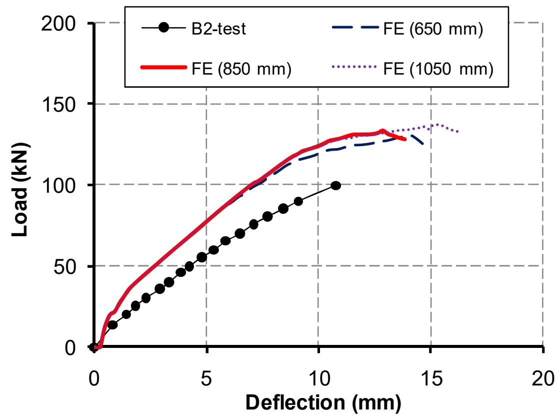

(a) Effect of the length of the CFRP sheets (1 layer)

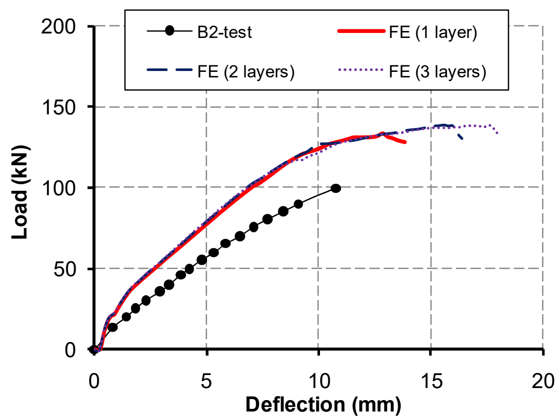

(b) Effect of the layers of the CFRP sheets (850 mm in length)

Figure 13. Effect of externally bonded horizontal CFRP sheets on the side surfaces of top and bottom chords

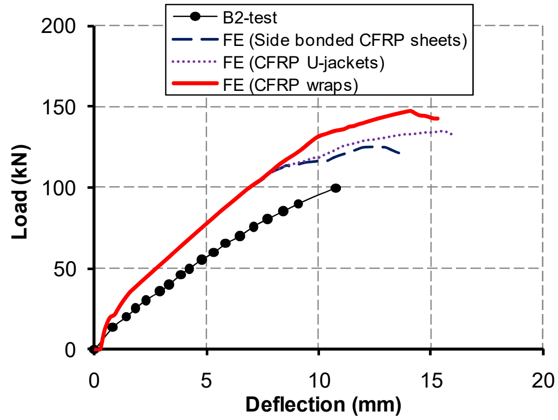

Figure 14. Effect of vertical side bonded CFRP sheets/CFRP U-jackets/CFRP wraps on the two sides of the opening

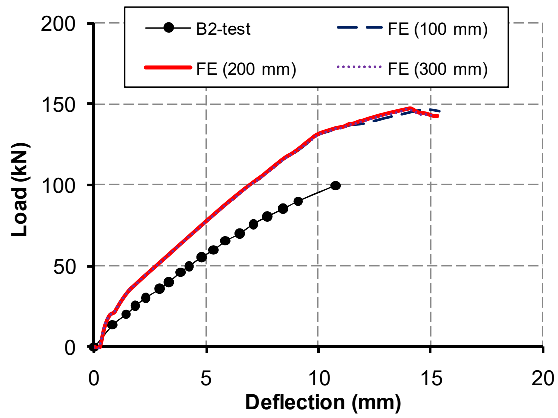

(a) Effect of the width of the CFRP wraps (1 layer)

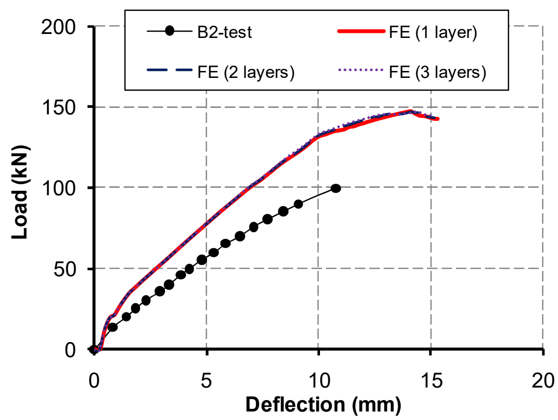

(b) Effect of the layers of the CFRP wraps (200 mm in width)

Figure 15. Effect of the CFRP wraps on the two sides of the opening

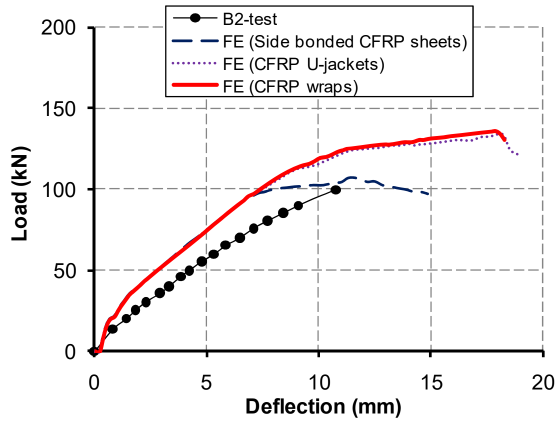

Figure 16. Effect of vertical side bonded CFRP sheets/CFRP U-jackets/CFRP wraps on the top and bottom chords

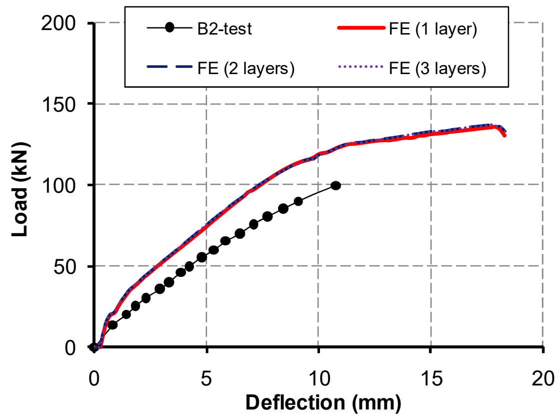

Figure 17. Effect of layers of the FRP wraps on the top and bottom chords

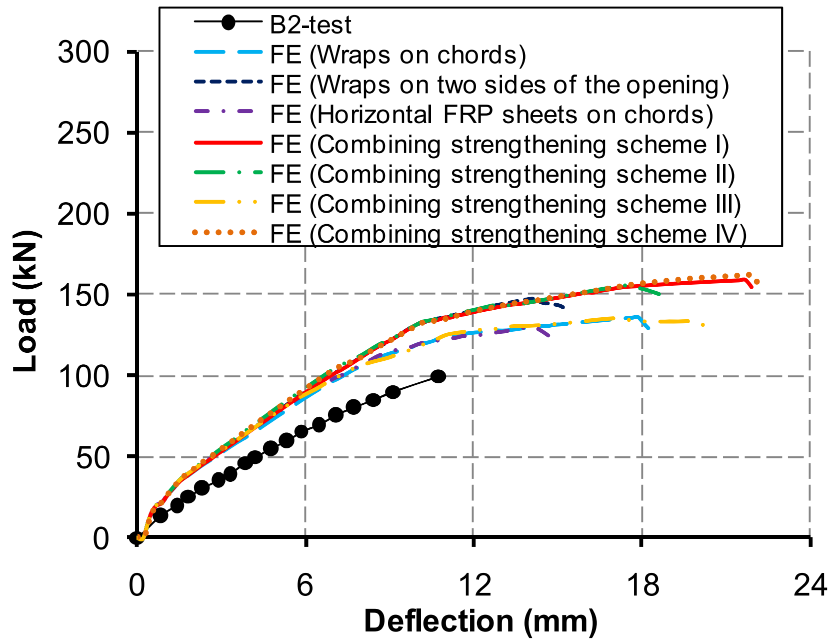

Figure 18. Combination of the strengthening schemes